# Surface dust redistribution on Mars as observed by the Mars Global Surveyor and Viking orbiters

Mark A. Szwast,[1] Mark I. Richardson,[1] and Ashwin R. Vasavada[2]

[1] The variation of surface dust coverage on Mars is mapped using Mars Global Surveyor (MGS) and Viking albedo data. Albedo is shown to correlate well with spectrally derived measurements of surface dust abundance and is subsequently used to gauge dust coverage. Atmospheric aerosols modify the albedo observed from orbit, complicating this analysis. However, opacity cycles are highly repeatable, and simultaneous, independent records of aerosol opacities are available to isolate their impact. The MGS albedo and imaging data contain global coverage on a daily basis, allowing the relationship between dust cover and specific meteorological events to be elucidated. The 2001 global dust storm produced the largest changes in surface dust coverage during the MGS mission. Other processes yielding significant changes include seasonal cap-edge winds, seasonally varying regional winds, local/regional dust storms, and extratropical cyclones. Dust devils and ongoing, small-scale dust lifting do not appear to significantly modify the global patterns of dust cover. Finally, we show that the apparent long-term darkening of the southern mid and high latitudes between the Viking and MGS eras is largely a consequence of the timing of image acquisition relative to global dust storms and surface dust "cleaning" by the seasonal ice cap; it does not represent a steady decadal-scale, secular change. In fact, following the 2001 global dust storm, in late southern spring, the southern hemisphere was brighter in MGS than in Viking data. This study reveals albedo to be a dynamic, climatological variable for Mars, similar to sea-surface temperature for terrestrial meteorology and climate.

**Citation:** Szwast, M. A., M. I. Richardson, and A. R. Vasavada (2006), Surface dust redistribution on Mars as observed by the Mars Global Surveyor and Viking orbiters, *J. Geophys. Res.*, *111*, E11008, doi:10.1029/2005JE002485.

## 1. Introduction

[2] The global distribution of dust and its redistribution through surface-atmosphere interactions are key factors in both Martian geology and climate. Deposition and removal of surface dust represent ongoing sedimentary geology [*Greeley et al.*, 1992], a continuation of aeolian processes responsible for the concentration of vast dust sheets [*Christensen*, 1986] and potentially for the thick sequences of sedimentary layered units identified by the Mars Orbiter Camera [*Malin and Edgett*, 2001]. Dust also plays a major role in moderating the global climate system [*Kahn et al.*, 1992]. Suspended in the atmosphere, dust modifies the transfer of visible and infrared radiation, affecting the heating rates of both the atmosphere and surface, and hence affecting the atmospheric circulation. Dust deposition on or removal from Mars' surface (which is typically darker than dust) will change its albedo and therefore daytime surface temperature and hence the vigor of local atmospheric convection. Icy surfaces may experience changes in albedo, absorption of solar radiation, and sublimation rate. The geographical distribution of surface dust has long been hypothesized to be a factor in determining the occurrence of (large) regional or global dust storms in a given year [*Haberle*, 1986; *Basu et al.*, 2004; *Pankine and Ingersoll*, 2004]. The atmosphere has a subseasonal timescale (i.e., memory) [*Richardson*, 1998; *Clancy*, 2000; *Liu et al.*, 2003; *Smith*, 2004], and as such, any inter-annual variability in the climate system that is not ascribable to stochastic atmospheric processes must involve changes in surface conditions.

[3] Albedo features were recognized on Mars as early as 1666 by Cassini [*McKim*, 1999]. During the 1900s, observers noted several multiyear variations in surface albedo patterns [e.g., *Sagan et al.*, 1972, 1973; *Veverka*, 1975, 1976; *Capen*, 1976]. Many of these changes were cyclic, in the sense that an area would darken and then brighten, or vice versa. Both Syrtis Major and Daedalia have shown this trend in the past. Before the Mariner 9 and Viking missions to Mars, one theory to explain albedo changes was biological activity [e.g., *Pollack et al.*, 1967]. More recently, surface changes have been attributed to the redistribution of fine, bright dust [e.g., *Sagan et al.*, 1972, 1973; *Veverka et al.*, 1974; *Lecacheux et al.*, 1991]. Global dust storms (GDS) raise large amounts of dust into the atmosphere of Mars, and occur frequently. Mariner 9 in 1971 was the first

[1]Division of Geological and Planetary Sciences, California Institute of Technology, Pasadena, California, USA.
[2]Jet Propulsion Laboratory, California Institute of Technology, Pasadena, California, USA.

to observe a GDS from Martian orbit. The Viking orbiters observed two GDS in 1977, while Mars Global Surveyor (MGS) observed the 2001 GDS. Since the first observation of a GDS in 1909, there have been at least 10 others in addition to hundreds of regional and local dust storms [*McKim*, 1999; *Cantor et al.*, 2001].

[4] Orbital observations of Mars' surface albedo and thermal emission, from the Viking Infrared Thermal Mapper (IRTM), the MGS Thermal Emission Spectrometer (TES), and the MGS Mars Orbiter Wide-Angle Camera (MOC-WA), together contain a global, multiyear, and multidecade record of Mars' surface layer. We use these data to investigate the degree to which surface dust deposits vary with the annual cycle and as a result of regional and global dust storms. The MGS mapping data extend over four Martian years at the time of writing, while the Viking data set provides a sampling of three northern summers/autumns and one southern summer/autumn. Together the data include three GDS's (two for Viking and one for MGS) and three large regional storms (one in the first MGS mapping year and two in the third).

[5] Previous studies of the IRTM data have indicated some variability in albedo. *Pleskot and Miner* [1981] examined the albedo data collected before, during, and after the twin 1977 global storms. Much of the observed variability was attributed to "transient brightenings," associated with dust storms, clouds, and surface frost. Indeed, many studies show that atmospheric dust strongly influences orbital measurements of albedo during periods of high dust loading. *Pleskot and Miner* [1981] found no systematic change in albedo before and after the global dust storms. *Christensen* [1988] reexamined the IRTM albedo data, focusing on separating temporal changes associated with the surface from those associated with the atmosphere. He also found that IRTM albedo data correlated with atmospheric dust loading. Variability of albedo within the Solis region (18−26°S, 81−89°W) apart from global storm periods was interpreted to indicate sporadic dust lifting. He concluded that water ice clouds did not appreciably influence measured albedos, suggesting minimal scattering when averaged over the broad 0.3−3.0-$\mu$m albedo channel. This observation indicates that the northern spring and summer, when dust loading is minimal, is the best time to perform interannual comparisons of surface albedo, even though water ice clouds are more frequent. *Christensen* [1988] found only one region that showed sustained changes in albedo following the global storms of 1977. Observations of Syrtis Major [7−17°N, 281−289°W] indicated that dust was deposited there during the decay phase of the global storms and was slowly removed thereafter. However, the sampling of the planet by IRTM was far from complete or systematic. Albedo changes associated with the 2001 GDS can now be assessed using the more complete data record available from TES.

[6] *Geissler* [2005] recently completed an image-based analysis of global and regional albedo changes between the Viking and MGS eras, and within the MGS era. He noted that all changes occurred on moderate to high thermal inertia surfaces, consistent with the deposition/removal of a thin dust layer over darker, more consolidated materials. He described several regional albedo changes in detail and offered hypotheses regarding the mechanisms involved, based on associations with prevailing winds, gusts, dust devils, dust storms, or active deposits of dark sand or silt. In addition, he noted a widespread darkening of the southern hemisphere that has occurred between the times when certain Viking and MGS imaging data were acquired. As with previous workers, Geissler notes that many albedo features on Mars have a cyclical behavior, though not correlated with seasonal cycles.

[7] In this paper, we document the redistribution of surface dust using the radiometric albedo data acquired by Viking IRTM and MGS TES, drawing additional information from other TES observables and MGS MOC-WA images. The central question of this paper is: by what mechanism(s) and in what manner has the atmosphere modified the surface distribution of dust? In the next section, we describe the data and processing methods. Where possible, we use data as archived in the Planetary Data System (PDS), without further refinement. In section 3 we discuss global properties in the context of observed storm events. In section 4, we examine the relationship between the MGS TES albedo and the Dust Cover Index (DCI) derived from thermal infrared spectra [*Ruff and Christensen*, 2002], and argue that albedo is a good metric of surface dust. In section 5, we describe changes in albedo that occurred during the MGS mission. We examine the spatial patterns of year-to-year changes and then focus in detail on specific regions. The effects of the 2001 GDS are especially evident. In section 6, we revisit the changes in albedo between the Viking and MGS missions described by previous workers, in light of new analyses of Viking and MGS albedo data. We are specifically interested in the timescale over which the changes occurred. Are major changes, such as the darkening of the southern hemisphere, indicative of a long-term, secular evolution of the dust distribution? Can we distinguish between the latter from more rapid variations, given the sparse record of observations? Finally, we examine the processes that lead to changes in surface dust coverage. A discussion highlights our findings and stresses the importance of surface dust as a climate variable, similar to air temperature or seasonal ice cap extent. Indeed, surface dust coverage (as indicated by albedo maps) is to the study of dust storm behavior on Mars as sea surface temperature maps are to the study of the El-Niño/Southern Oscillation (ENSO) on Earth.

## 2. Data and Processing

[8] We acquired TES Lambert albedos from the PDS and used them without further refinement. The TES Lambert albedos were measured using a bolometer sensitive over a visible to near-infrared passband of 0.3−2.9 $\mu$m. The calculation of Lambert albedo from the bolometer measurements is described by *Christensen et al.* [2001]. Lambert albedos (hereafter referred to as albedo) provide a measure of surface reflectivity that is independent of the solar zenith angle. The TES albedos are not corrected for atmospheric scattering; they are a measure of the net reflectivity of the surface and the atmosphere. We use albedos only from the MGS mapping orbits. These sun-synchronous, near-polar orbits, combined with the nadir-pointed instruments, resulted in excellent spatial coverage and low incidence and emission angles. The TES footprint is a square with

dimensions of approximately $3 \times 3$ km [*Christensen et al.*, 2001] (uncompensated smearing during the course of each observation tends to elongate the footprint into a rectangle, however).

[9] The IRTM measured albedo using a wavelength range and sensor similar to TES [*Pleskot and Miner*, 1981]. These data also were acquired from the PDS and used without refinement. The orbits and observational strategies of the Viking orbiters resulted in data acquisition over a wide range of incidence and emission angles. High emission angles influence the derived albedo of the target surface. We consider this effect below, but unless otherwise stated, an emission angle constraint of $60°$ was used. The IRTM footprint size varied during the spacecrafts' eccentric orbits between roughly tens and many hundreds of kilometers.

[10] Imaging data from the MOC-WA provides an alternate means of assessing surface albedo, at least in a qualitative sense [*Caplinger and Malin*, 2001; *Malin and Edgett*, 2001]. The MOC-WA red-channel images provide an independent confirmation of the TES results. In addition, the higher spatial resolution of these data ($\sim$250 m pix$^{-1}$) and their regular acquisition provide some geological and topographical context, and sometimes reveals information about the processes involved (e.g., presence of dust devils or wind streaks). The MOC-WA data are taken from the PDS and calibrated and mapped using the USGS ISIS package.

[11] Throughout our study we relied upon ancillary data to interpret the albedo and understand sources of error. Such data include dust and ice infrared opacities [*Smith*, 2004], daytime surface temperatures (derived from the peak brightness temperature), and daytime air temperatures. The latter were generated by applying the IRTM T15 weighting function to the TES spectra in the 15-$\mu$m region using the "vanilla" code accompanying the TES PDS data set [*Liu et al.*, 2003]. All data are available from the PDS archive.

[12] Much of our analysis was facilitated by organizing the TES and IRTM data into a four-dimensional array of latitude, longitude, $L_s$, and property value (e.g., albedo). We collected the data in bins of $1°$ in latitude by $1°$ in longitude by $10°$ of $L_s$. In addition, we calculated the number of measurements in each bin and their sum. The TES and IRTM data were binned separately, as were each year. For maps that required a spatial bin size larger than $1°$ (e.g., due to sparse data), all measurements in each of the $1°$ bins were used in calculating the new average. This procedure produces the same result as binning the original data directly into the larger bins. When calculating the zonal mean, global mean, or area mean, only the averaged values of each $1°$ bin were used, in order to reduce bias due to variations in zonal coverage. Empty bins were not included in the mean calculations. For line plots averaging over areas larger than $1°$ in latitude, bin values are weighted by the true surface area of each bin. For maps with a spatial bin size of less than $1°$, the PDS data were binned using the appropriate bin dimensions.

## 3. Overview of Atmospheric Behavior During MGS

[13] Here we provide a summary of the major atmospheric events that occurred during the MGS era. The MGS mapping mission has covered over three Mars years and captured several regional dust storms, one GDS [*Cantor et al.*, 2001; *Liu et al.*, 2003; *Smith*, 2004; *Strausberg et al.*, 2005], and numerous periods of dust devil activity [*Balme et al.*, 2003; *Fisher et al.*, 2005].

[14] Figure 1 shows the latitudinal and seasonal variations (with $1°$ $L_s$ resolution) of key quantities. The surface temperature panel is a metronome of the seasonal cycle, highlighting the seasonal displacement of the subsolar latitude and the greater intensity of southern summer. The panel also reveals a subseasonal cooling anomaly just after the middle of the second year ($L_s = 200°$). The air temperature panel shows increased variability during each southern spring and summer (Figure 1b). The surface cooling event in year two is correlated with the largest warming event in the air temperature data. Smaller air temperature warming events can be found in the first year and third year. Each of these events is associated with a spike in dust opacity (Figure 1c), corresponding to a dust storm.

[15] The opacity data indicate storm activity beyond that identifiable in the air temperature data. During the first mapping year, storms are evident near the southern seasonal cap edge just before $L_s = 180°$, in both hemispheres at about $L_s = 225°$ (this is the inter-hemispheric "Chryse" or "flushing" storm that began in the northern high latitudes as a frontal dust cloud, as described by *Cantor et al.* [2001] and *Wang et al.* [2003]), and northern high-latitude (again, mainly frontal) storms between $L_s = 330°$ and $360°$. In the second mapping year, a global storm began just before $L_s = 180°$, starting with regional activity in Hellas and spreading to the east [*Smith et al.*, 2002; *Strausberg et al.*, 2005]. Secondary dust lifting centers were observed in the Daedalia/Solis region. A northern hemisphere storm was again observed at roughly $L_s = 345°$ and associated with fronts. The third mapping year resembled the first to some degree. A dust storm occurred in the southern high latitudes near $L_s = 180°$ (dust storms happened every year at these latitudes and season, but led to a global storm only in year 2). Large, flushing storms (beginning in high northern latitudes as fronts and moving quickly across the equator) occurred at $L_s = 225°$ and $310°$, in both of the seasonal windows identified by *Wang et al.* [2003]. A modest, high-northern-latitude event occurred at roughly $L_s = 25°$ in year 4. Data from the southern spring and summer of year 4 (starting March 2005) had not been obtained at the time of writing.

[16] Water ice opacity follows a highly repeatable cycle (Figure 1d). Substantial clouds appear in the tropical atmosphere, between roughly $10°S$ and $30°N$ [*Clancy et al.*, 1996; *James et al.*, 1996; *Pearl et al.*, 2001] between roughly $L_s = 30°$ and $160°$ (the range depends on a subjective opacity threshold used to define the presence and absence of cloud) [*Wang and Ingersoll*, 2002; *Liu et al.*, 2003; *Smith*, 2004]. Clouds forming part of the northern polar hood in northern autumn and winter can also be seen in Figure 1d.

[17] The impact of dust and ice opacity on albedo can be assessed by comparing Figures 1e and 1f with Figures 1c and 1d. Both the zonal mean albedo and the deviation from the average zonal mean albedo (averaged over the entire TES data set) are shown; the latter removes the hemispheric albedo dichotomy and highlights temporal changes. Dust opacity has a significant impact on the zonal-mean albedo,
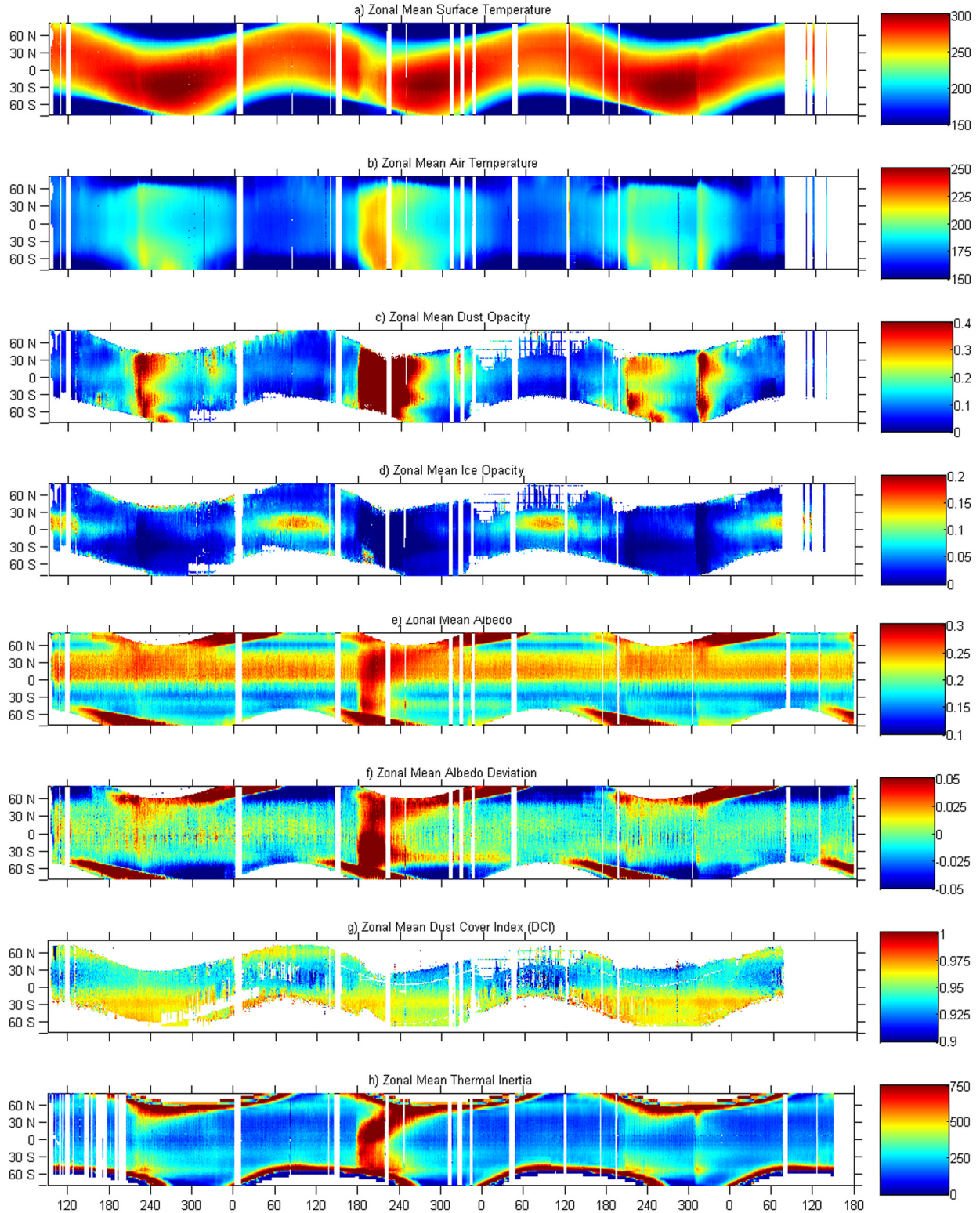
**Figure 1.** Zonal means of selected TES measurements as functions of latitude and $L_s$. The data are binned by $1°$ of latitude and $1°$ of $L_s$ and extend over three Mars years. The panels show (a) daytime ($\sim 2$ pm) surface temperature, (b) daytime air temperature, (c) dust infrared opacity, (d) ice infrared opacity, (e) albedo, (f) albedo deviation from annual average, (g) dust cover index, and (h) thermal inertia.
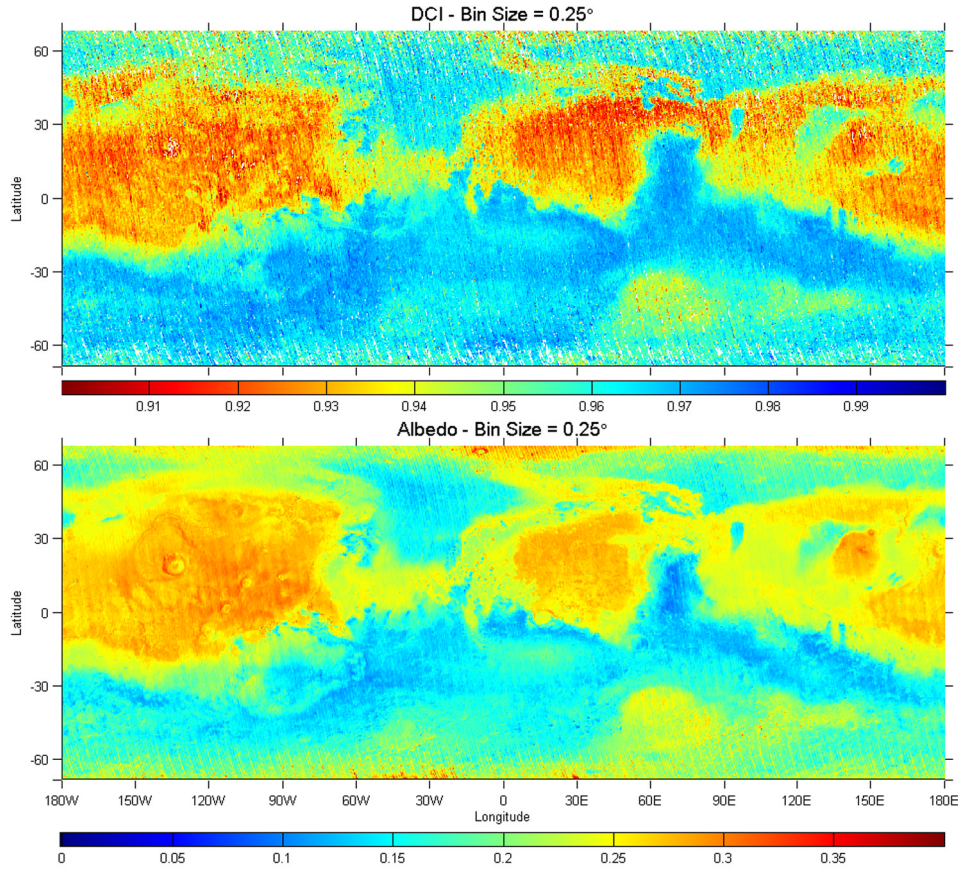
**Figure 2.** Comparison of TES (top) dust cover index with (bottom) albedo. Both are binned by 0.25° of latitude and 0.25° of longitude and averaged over multiple years.

especially during the global storm of 2001. Lesser signatures of the large regional storms of the first and third mapping years can also be seen. The cycle of cloud ice opacity is not accompanied by an obvious change in albedo, although a very slight brightening (∼0.01) can be seen in the albedo deviation (Figure 1f) in each of the northern spring/summers and just north of the equator. The effect is much smaller than that associated with the major dust storms, and like the clouds themselves, is essentially repeatable from year to year (interannual comparisons can therefore be designed to negate any cloud effect).

## 4. Is Albedo a Good Gauge of Surface Dust Coverage?

[18] High albedo is widely believed to indicate enhanced coverage of the surface by dust. If so, one can map the dust distribution by mapping the areas of high albedo [*Christensen*, 1986, 1988]. This interpretation is supported by several lines of evidence, including the association of high albedo with low thermal inertia, and the relative albedos of dust, rocks, and soils observed by landers. An alternate means of mapping fine-grained silicates (such as dust) that exploits thermal infrared spectra rather than broadband visible albedo data has been developed by *Ruff and Christensen* [2002]. The Dust Cover Index (DCI) takes advantage of a transparency feature associated with silicate particles with radii ≪100 $\mu$m and located at the short-

wavelength end of the TES spectra. The DCI is defined as the average emissivity between 1350 and 1400 cm$^{-1}$. The DCI is sensitive over a depth of a few tens of microns, rather than the few microns for albedo. However, for dust deposits of several particle thicknesses or greater, DCI and albedo should agree if both are good gauges of the true dust coverage.

[19] The albedo and DCI for the full MGS mapping-orbit mission are shown in Figure 2. The DCI data were extracted from the TES archive using the quality constraints suggested by *Ruff and Christensen* [2002], with the exception that a minimum surface temperature of 250 K (rather than 260 K) was used. *Ruff and Christensen* [2002] report a good gross agreement between the data sets, but highlight regions in Arabia and elsewhere where a boundary exists between high and very high albedo that is not reflected in the DCI (but interestingly, usually is reflected in the thermal inertia). As our maps also show, these are the only significant differences between DCI and albedo. Detailed comparison of our maps (e.g., blinking) demonstrate that there are no regions of high or low albedo that are not simultaneously regions of low or high DCI, respectively (low DCI corresponds to high dust cover and high albedo). The origin of the discrepancy between albedo and DCI at very high albedo is unknown. *Ruff and Christensen* [2002] speculate that it may be associated with a saturation of the DCI for surfaces that are not completely dust covered, such that some range of albedo at the very highest values can be admitted by the same DCI. That the brightest surfaces
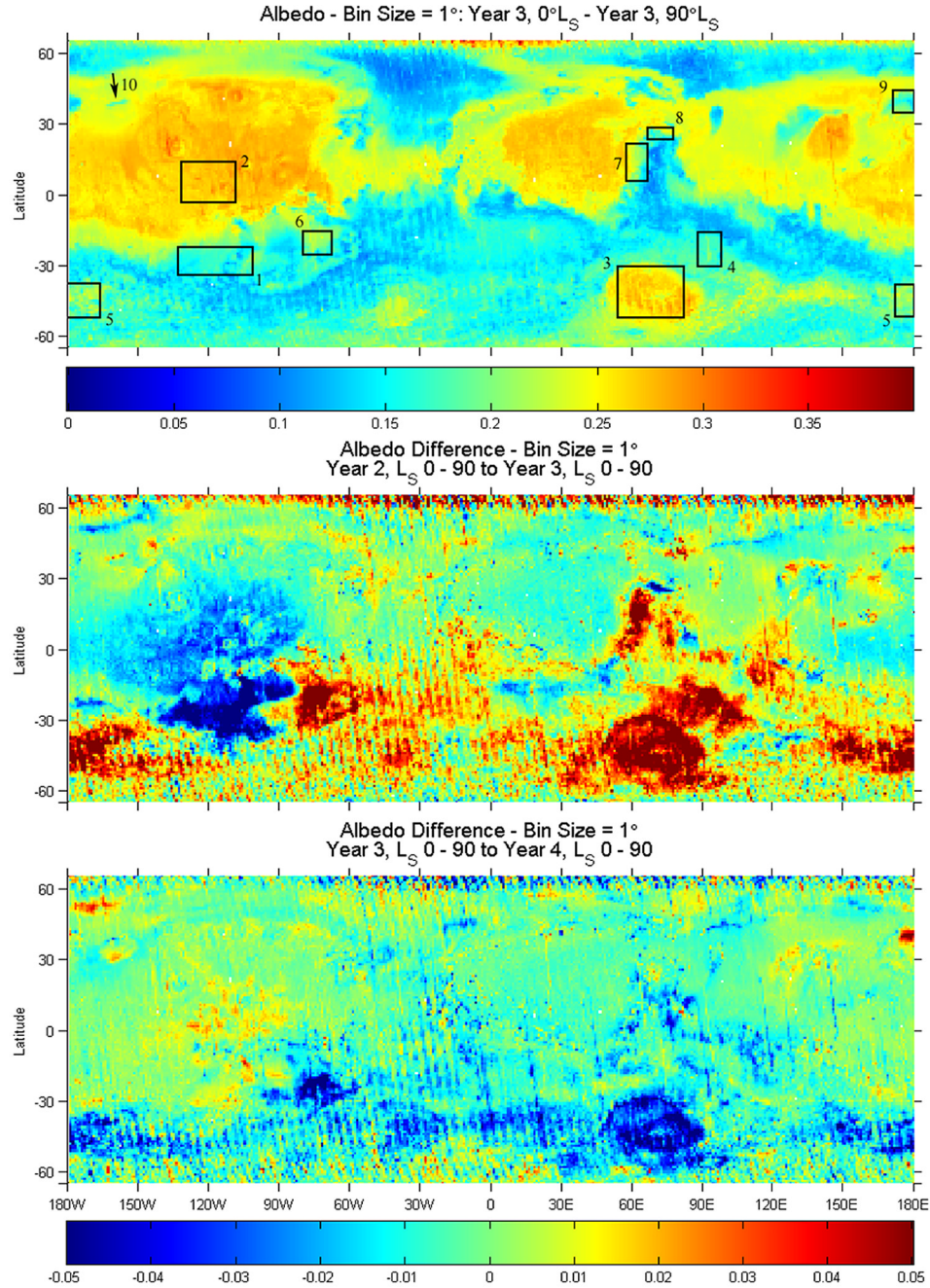
**Figure 3.** TES albedo and year-to-year difference maps. All data are binned by 1° of latitude and 1° of longitude and averaged over the period $L_S$ 0°–90°. The panels show (top) albedo in Year 3, (middle) change in albedo Year 3 minus Year 2, and (bottom) change in albedo Year 4 minus Year 3. The numbered boxes in the albedo map are our regions of interest (section 5).

should also correspond to low thermal inertia (characteristic of depths of many centimeters) supports the idea of thick dust continents. The remarkable agreement between DCI and albedo validates the use of albedo as a measure of surface dust coverage.

## 5. Dust Redistribution During the MGS Mission

[20] The most dramatic atmospheric dust event of the MGS mission to date was the 2001 GDS (Figure 1). A natural place to begin looking for the influence of the atmosphere on the surface dust distribution is the period encompassing this storm. Figure 1 suggests that the atmospheric dust opacity influences the albedo, but its effects are minimal during northern spring. In Figure 3a we show the albedo during northern spring ($L_s = 0°–90°$) of the third mapping year (the spring following the 2001 storm). Figure 3b reveals the difference in albedo between years 2 and 3 (as averaged over northern spring). While some noise is apparent, especially in the northern high latitudes (associ-

ated with the seasonal ice cap and hood), spatially coherent regions of significant albedo change can be identified. These changes do not result from biases in the data collection (for example, data volumes peaking during different periods of the seasonal window in the two years and swamping the signal), as subbinning by $10°$ of $L_s$ was employed (see section 2). In addition, maps created using shorter seasonal windows show nearly identical features.

[21] A broad swath of the surface in the southern mid-latitudes, and across Hesperia and Syrtis in the tropics, shows significant net brightening, with albedo enhancements of between 0.02 and 0.05. A smaller fraction of the surface darkens, with the only significant geographical concentration in a contiguous region including Tharsis, Daedalia, and Syria. Very slight darkening ($\sim$0.01) of high-albedo areas of Amazonis, Elysium, and Arabia is also evident.

[22] If brightening of the surface is taken to represent net gain of surface dust in a given region, then a somewhat surprising result follows from Figure 3b. Hellas, which was the site of initiation of the 2001 storm and apparently an active dust-lifting center well into the storm evolution [*Strausberg et al.*, 2005], was actually a net sink for dust over the life cycle of the storm. On the other hand, if darkening is taken to indicate net loss of surface dust, then the Daedalia/Syria region, which the MOC and TES opacity data suggest was an important secondary lifting center for the storm [*Liu et al.*, 2003; *Strausberg et al.*, 2005], was in fact the only major net dust source. The interpretation of darkening as net loss of surface dust and vice versa is examined in greater detail in the following sections.

[23] Albedo differences between the third and fourth mapping years are shown in Figure 3c. Broadly speaking, areas of darkening in Figure 3c grossly correspond to areas of brightening in Figure 3b, but there are a number of exceptions. In fact, this compensation is only really complete in Hellas and across the southern midlatitudes between about $35°S$ and $55°S$, with darkening of between 0.03 and 0.05. If the relationship between albedo change and net dust deposition outlined above holds, then comparison of Figures 3b and 3c suggests some cyclicality in surface dust redistribution, at least in these latitudes. More equatorward, the areas darkened by the storm are not brightened sufficiently to return albedos to prestorm levels. Most significantly, the putative net 2001 storm dust source region of Tharsis/Daedalia brightens by only as much as 0.01 on large scales, compared with a darkening over the previous year of 0.04–0.05, and many areas of the source region do not brighten at all.

[24] Maps of DCI show broadly similar year-to-year variability of surface dust as the albedo maps (Figure 4), providing support for the interpretation of albedo differences as representative of changes in the amount of surface dust coverage. The year 3 mean DCI map shown in Figure 4 differs from that in Figure 2 in the choice of seasonal date: the latter was generated from data collected in late southern spring and summer in order to highlight southern midlatitudes before and after the storm (only in these seasons are surface temperatures sufficiently high to allow valid DCI values to be calculated for these latitudes). The year 1-year 2 difference (corresponding to before and after the storm for these seasonal dates) is similar to the second panel of

Figure 3 (note reversal of color bar), but considerably noisier. Through this noise, only the strongest of the surface dust coverage changes evident in the albedo data can be seen. These include the lessening of surface dust coverage in Daedalia and southern Tharsis (Syria and Sinai), and the increase in surface dust coverage in Hellas, Hesperia, Solis, Sirenum, and Argyre. There is some hint of the increased surface dust in southern Syrtis, but the DCI differences become very noisy at these northern tropical latitudes. The differences resulting from the passage of the following year also echo those in the albedo record. Hellas and Argyre are seen to experience net loss of surface dust, while there is some hint of resupply over Daedalia and southern Tharsis. In general, where signatures in the DCI year-to-year changes emerge from the noise, they are consistent with the largest of the changes seen in the albedo data, suggesting again that DCI and albedo are telling the same story, with albedo relaying that story with greater clarity and detail. Due to the greater volume of high-quality albedo data, we use it instead of DCI for the remainder of this study.

[25] While the maps provide very clear patterns of albedo change and an enticing picture of the dynamics of surface dust redistribution, their temporal resolution is coarse (1 Mars year). In the following sections we examine ten Regions of Interest (ROI) in greater detail, with a temporal resolution of $10°$ of $L_s$. The ROIs in Figure 3a were selected on the basis of the more extreme regional variations noted in our global maps, but the behaviors are representative of many other locations. Albedo variations of many of these regions have been documented in the past [e.g., *Capen*, 1976; *Bell et al.*, 1999; *McKim*, 1999; *Geissler*, 2005]. The number of the ROI (indicated in Figure 3a) corresponds to the subsection number below.

## 5.1. Daedalia Planum

[26] The Daedalia region has a long record of albedo changes. *Capen* [1976] called the 1973 darkening of the region "the most significant change observed on Mars" since the 1950s. A number of changes in the region from the record of telescopic observation are reported by *McKim* [1999]. Long-term differences between Viking images and both Hubble Space Telescope [*Bell et al.*, 1999] and MGS data [*Geissler*, 2005] show a substantially brighter Daedalia in 1997 and in 1999–2001, respectively.

[27] The variations of albedo and selected other variables over the course of the four MGS mapping years for Daedalia ($23°S$–$34°S$, $101°W$–$132°W$) are shown in Figure 5. From $L_s = 110°$ in year 1 to this same seasonal date in year 2, the albedo shows a slow variation of roughly 0.01 amplitude (on a mean value of about 0.225) and a period of one Martian year. This seasonal cycle in derived albedo may be due to (1) variations in the dust cover, (2) variations in atmospheric dust or water ice opacity that corrupt the measurement of surface albedo, or (3) a different systematic error in the albedo derivation. Without any reason to suspect a seasonal cycle in dust coverage, we discard the first explanation. While the variation of dust opacity does have some influence on the Daedalia albedo in the first complete year, the effect is not strong. The opacity data do have a cyclic pattern roughly in phase with the albedo data, but they also exhibit a major perturbation
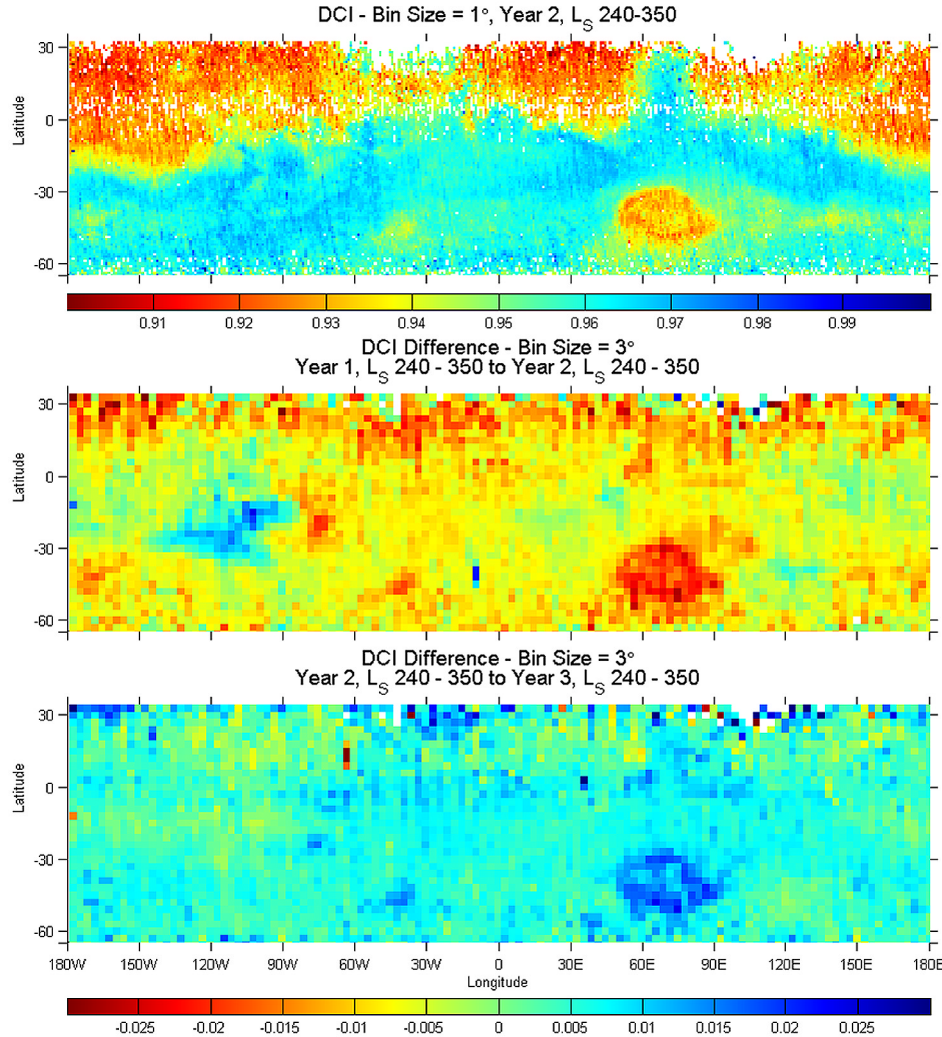
**Figure 4.** TES dust cover index (DCI) and year-to-year difference maps. All data are binned by 1° of latitude and 1° of longitude and averaged over the period $L_s$ 240°−350°. The panels show (top) DCI in Year 2, (middle) change in DCI Year 2 minus Year 1, and (bottom) change in DCI Year 3 minus Year 2.

associated with the "cross-equatorial flushing dust storm" of 1999 [*Cantor et al.*, 2001; *Wang et al.*, 2003]. There is no corresponding perturbation in the albedo data, suggesting an insensitivity of derived albedo to atmospheric dust opacity (which is expected at high-albedo sites). The atmospheric cloud ice opacity also exhibits a seasonal cycle, but one that is nearly 180° out of phase with that of albedo. Conversely, the dust and ice opacities have a substantial impact on the derived thermal inertia, explaining essentially all of the seasonal variation and higher-frequency perturbations. Ruling out dust and water ice opacity, we suspect a systematic error in the albedo retrieval due to the assumption of a Lambertian reflectance phase function for the surface. Daedalia is located on the southern tropic. The incidence and phase angles are smallest at southern solstice and largest at northern solstice, such that a reflectance phase function slightly skewed toward zero phase (rather than Lambertian) could explain the apparent seasonal albedo cycle.

[28] The largest signal in the Daedalia albedo data is a roughly 0.06 drop across the 2001 GDS. Following the storm (after roughly $L_s = 240°$ in the second mapping year), the albedo remains near a value of 0.17, again executing a small seasonal cycle. After examining the period between $L_s = 330°$ and $L_s = 90°$ in the final two years of observations, one may argue that a year after the GDS, the albedo increased by 0.005−0.01. The thermal inertia values away from the major storms do not show any significant year-to-year variability, and no transition associated with the 2001 storm. If the albedo offset associated with the storm is due to dust cover change, then the lack of change in thermal inertia suggests that the thickness of dust removed from the surface is less than a few centimeters but more than a few microns.

[29] As valuable as quantitative measurements of albedo and thermal inertia are, it is interesting to visualize the changes on the surface in the MOC WA images, specifically those taken as Daily Global Maps (DGM). Figure 6 shows a portion of the Daedalia ROI imaged just before the 2001 storm and one Martian year later (the images actually cover a region extending about twice as far in latitude as the albedo ROI, but including only the eastern half of the ROI).
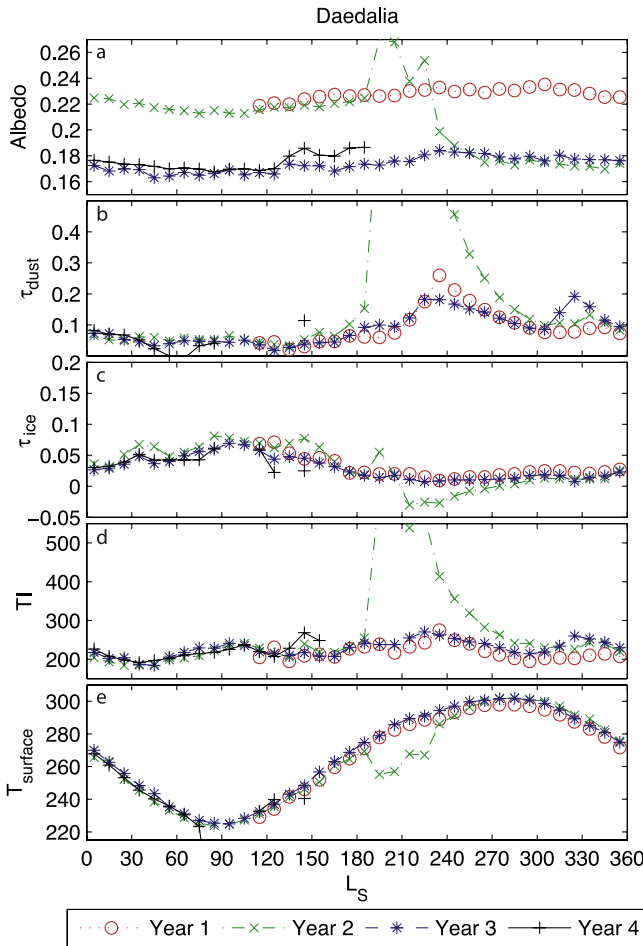
**Figure 5.** Selected TES measurements averaged over our Daedalia region of interest (23°S–34°S, 101°W–132°W) binned by 10° of $L_s$. The panels show (a) albedo, (b) dust infrared opacity, (c) ice infrared opacity, (d) thermal inertia, and (e) daytime (~2 pm) surface temperature. Each plot shows the entire time series of TES measurements to date. The colors and symbols change at the year boundaries from red circles (Year 1) to green crosses (Year 2) to blue asterisks (Year 3) to black pluses (Year 4).

The figure shows that the region is generally darker in the second frame, but that there are distinct spatial patterns to this darkening. The large, medium-bright region indicated by arrows 1 and 2 is largely absent in the second frame. Only a very small fraction of the area remains somewhat bright, near arrow 2. The area around arrow 3 is quite uniformly medium-bright in the first frame, but has become partially darkened in the second, with a distinct boundary forming between the still bright region to the upper left and the darkened region to the lower right. The area to the north and west of arrow 4 has darkened sufficiently in frame 2 that the boundary of the bright region indicated by the arrow in frame 1 has largely been removed. Interestingly, the small area to the immediate south of arrow 4 and the area pointed to by arrow 6 actually brighten between the two frames, showing the opposite trend of the area as a whole. The region pointed to by arrow 5 does not change significantly between the two years. While the images were processed so

as not to introduce image-to-image brightness differences, MOC images do not have high radiometric accuracy (10% absolute, 3% relative [*Malin et al.*, 1992]). However, the area indicated by arrow 5 is also unchanged in the TES albedo data (compare the second frame of Figure 6 with the Figure 3a). We are confident that the MOC WA images provide a higher-resolution view of the patterns contained in the TES albedo data.

[30] Images from the GDS period contain evidence for dust activity in the ROI, specifically removal of dust from the surface. *Strausberg et al.* [2005] identify convective or sharp, "clumpy" dust cloud top structures with dust lifting. In Figure 7, MOC DGM images at roughly 3.8 km/pixel for the Daedalia, Syria, and Sinai (Tharsis) regions show the initiation of dust lifting within the secondary lifting center of the 2001 storm. The correlation of these unusually thick dust clouds in the Daedalia and Tharsis regions, which appear as areas of net darkening in the albedo data, is of circumstantial importance in itself. In addition, the highest-resolution images of the secondary lifting center initiation show some evidence of actual lifting plumes feeding the cloud, suggesting that the dust observed in the atmosphere is locally derived, resulting from net lifting of dust from the surface.

### 5.2. Tharsis

[31] Observations over the Tharsis ROI (0°N–20°N, 90°W–120°W) are shown in Figure 8. During the first complete Martian year of mapping, the trend in albedo is essentially flat between about $L_s = 180°$ and the following $L_s = 60°$. Every year has elevated albedo over a period centered at $L_s = 110°$. The shape of the seasonal albedo trend is different from that at Daedalia, and appears most similar to the trend in atmospheric water ice opacity. The peak values of ice opacity at Tharsis are about three times greater than at Daedalia, in agreement with images that show widespread cloud over the Tharsis volcanoes in northern spring and summer [e.g., *Wang and Ingersoll*, 2002]. The dust opacity has essentially no impact on the Tharsis albedo trend, likely because the atmospheric dust is of similar brightness to the surface material.

[32] As with Daedalia, the largest signature in the Tharsis albedo history is the drop in brightness across the 2001 GDS. This drop is smaller than that at Daedalia (about 0.03 vs. 0.06). The albedo at Tharsis appears to steadily increase following the 2001 storm, suggesting a slow return of dust lost during the storm (or slow removal of dust if the GDS deposited dust that is darker than the Tharsis surface). The thermal inertia shows no consistent year-to-year differences, suggesting no centimeter-deep changes in dust cover.

### 5.3. Hellas

[33] The albedo trend in the Hellas basin (31°S–53°S, 54°E–82°E; Figure 9) is influenced by a process not active within the two previous ROIs: seasonal ice cap formation. From roughly $L_s = 70°$ to about $L_s = 170°$ the Hellas ROI is partially covered by ice, yielding an increase in albedo. In the ice-free southern spring and summer, the albedo trends to lower albedo values toward the end of each year. Jumps in albedo correspond with dust storm events in the dust opacity plot. The seasonal cap edge storm activity around southern spring equinox and the larger regional and global
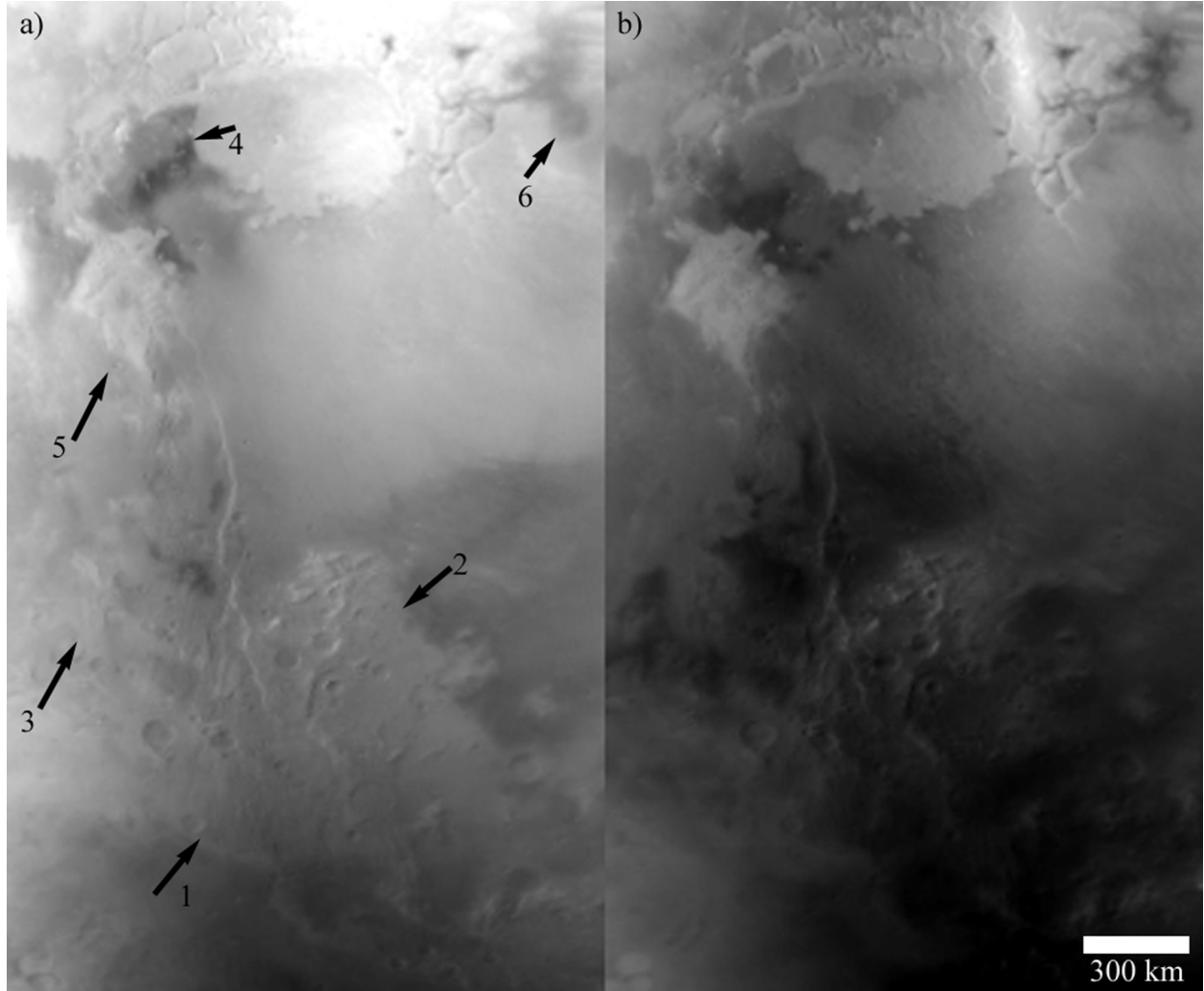
**Figure 6.** MOC WA DGM showing part of our Daedalia region of interest. Figure 6a was taken shortly before the 2001 global dust storm. Figure 6b was taken approximately one Mars year later. For the meaning of the numbered arrows, see text in section 5.1.

storms are identifiable in both the albedo and dust opacity records. The general decline of dust opacity from southern spring into late southern summer is responsible for the overall decline in albedo values during this same period. The low elevation of Hellas results in high total column dust opacities. Cloud ice opacities are low during the periods they can be derived, except for near winter solstice. At no time do they appear to significantly influence the albedo.

[34] Despite the variations due to atmospheric dust and the seasonal ice cap, a clear signature of year-to-year change in albedo is evident. Following the spike of albedo during the 2001 GDS, the albedo of Hellas relaxes to a value about $0.06-0.08$ higher than during the same seasonal dates in the prior year (a >30% increase from values near $0.18-0.2$). This elevated albedo persists throughout the year following the 2001 storm until the development of the seasonal ice cap shrouds the surface. When the veil of winter ice is lifted after $\sim L_s = 170°$, the albedo is similar to that in the first mapping year. For much of the rest of the southern spring and summer, year 3 resembles year 1, other than the effects of dust storms. However, after the second large storm of year 3, the albedo remains about 0.01 higher than the first mapping year.

[35] The most surprising aspect of the Hellas albedo trend is the net brightening of the surface. This implies that Hellas was a net sink for dust over the 2001 GDS, despite the fact that it is the acknowledged site of storm initiation [*Smith et al.*, 2002; *Strausberg et al.*, 2005]. Figure 10 shows the brightening of Hellas at moderate resolution using MOC WA DGM images from mid southern summer. The images demonstrate that the brightening corresponds to deposition of dust on formerly darker areas within the central, southern, and eastern parts of the basin. While many darker areas can be seen in the year 1 image, the images from year 2 (just following the storm decay) show only a few, with the basin albedo more uniform and brighter than before. Two images taken about a week apart are shown to demonstrate that the general brightening is due to surface dust rather than atmospheric haze. While the edge of the bright material at the basin rim is complex in shape (especially on the northwestern rim), the patterns are identical and hence are not due to transient cloud or dust haze. This is consistent with derivation of constant dust and water ice opacity at this season (Figure 9). The tendency of the northwestern portion of Hellas to brighten less than the remainder is consistent
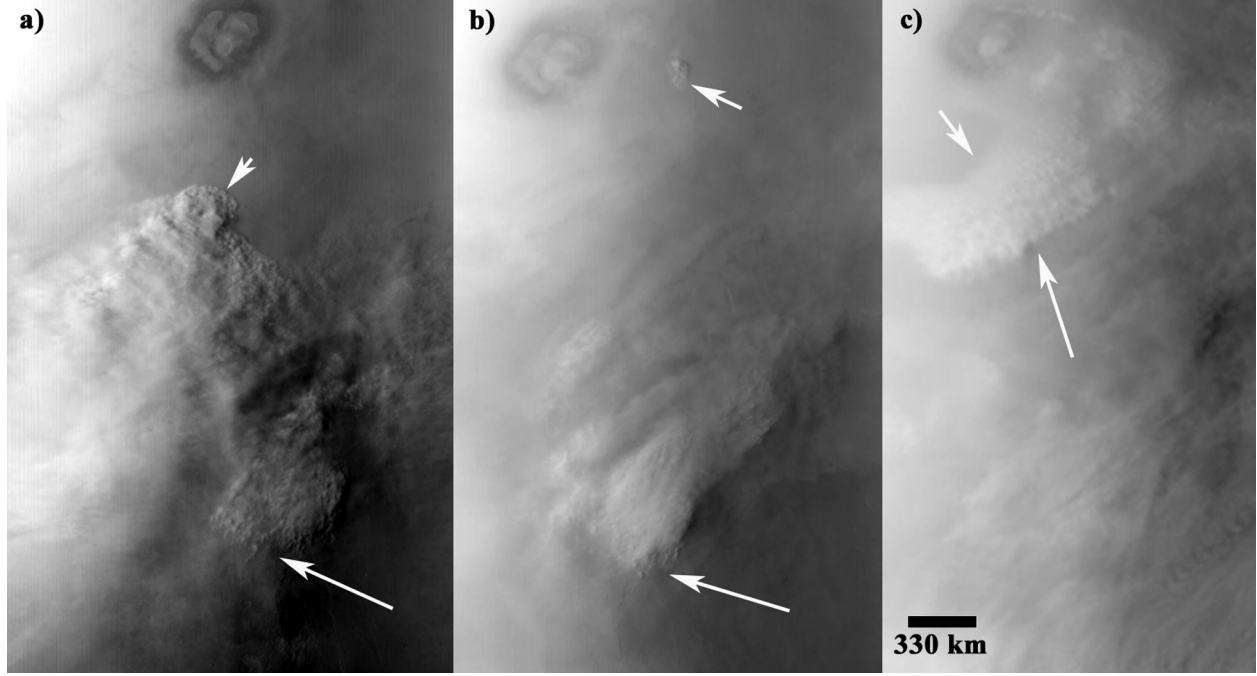
**Figure 7.** MOC DGM images (~3.8 km/pixel) of dust lifting in the secondary lifting centers of the 2001 global dust storm: (a) Daedalia, (b) Syria, and (c) Sinai (Tharsis). Arrows indicate areas of suspected active dust lifting.
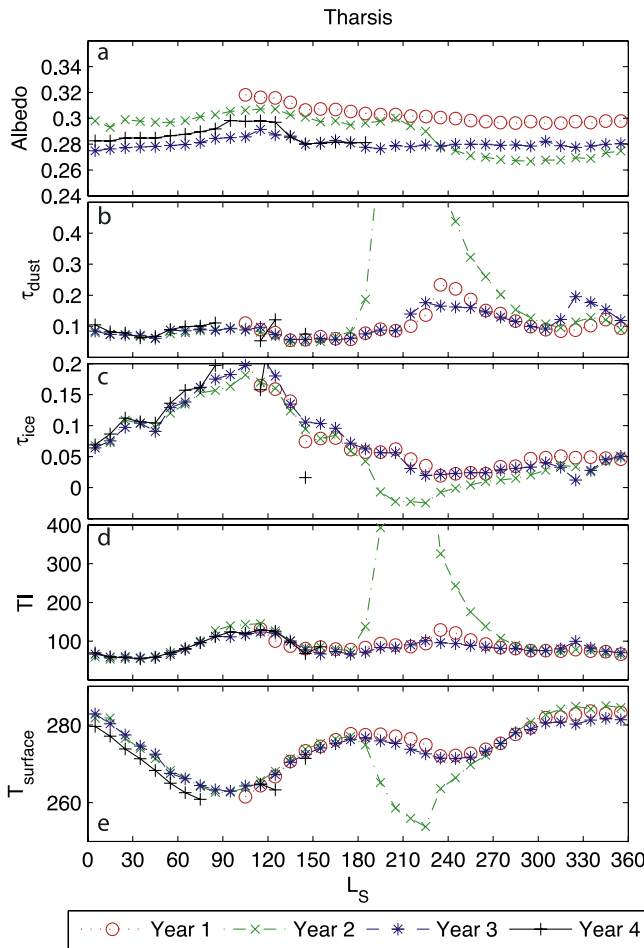


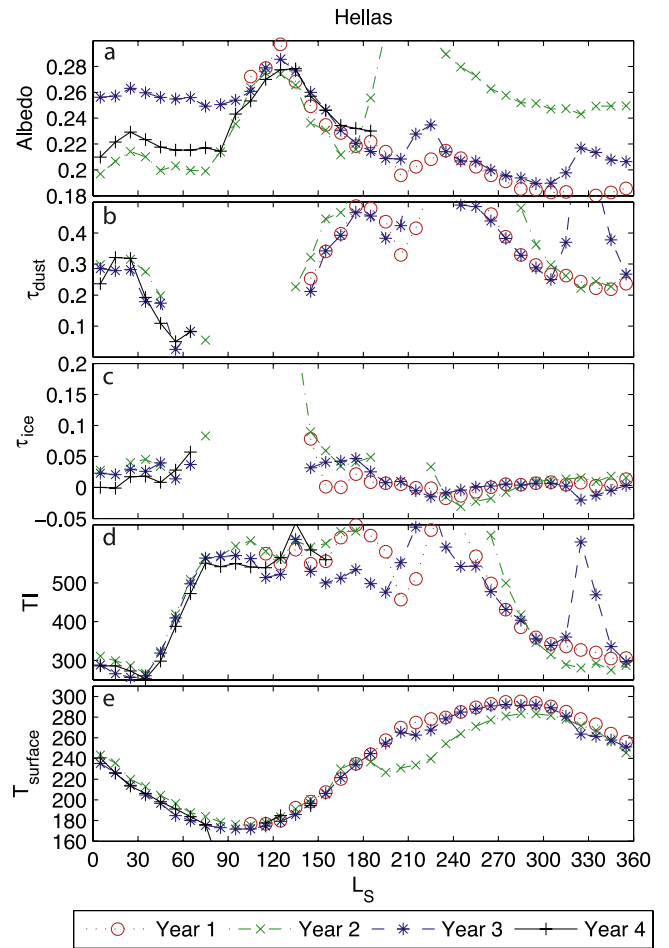**Figure 8.** Similar to Figure 5 for our Tharsis region of interest (0°N–20°N, 90°W–120°W).

**Figure 9.** Similar to Figure 5 for our Hellas region of interest (31°S–53°S, 54°E–82°E).
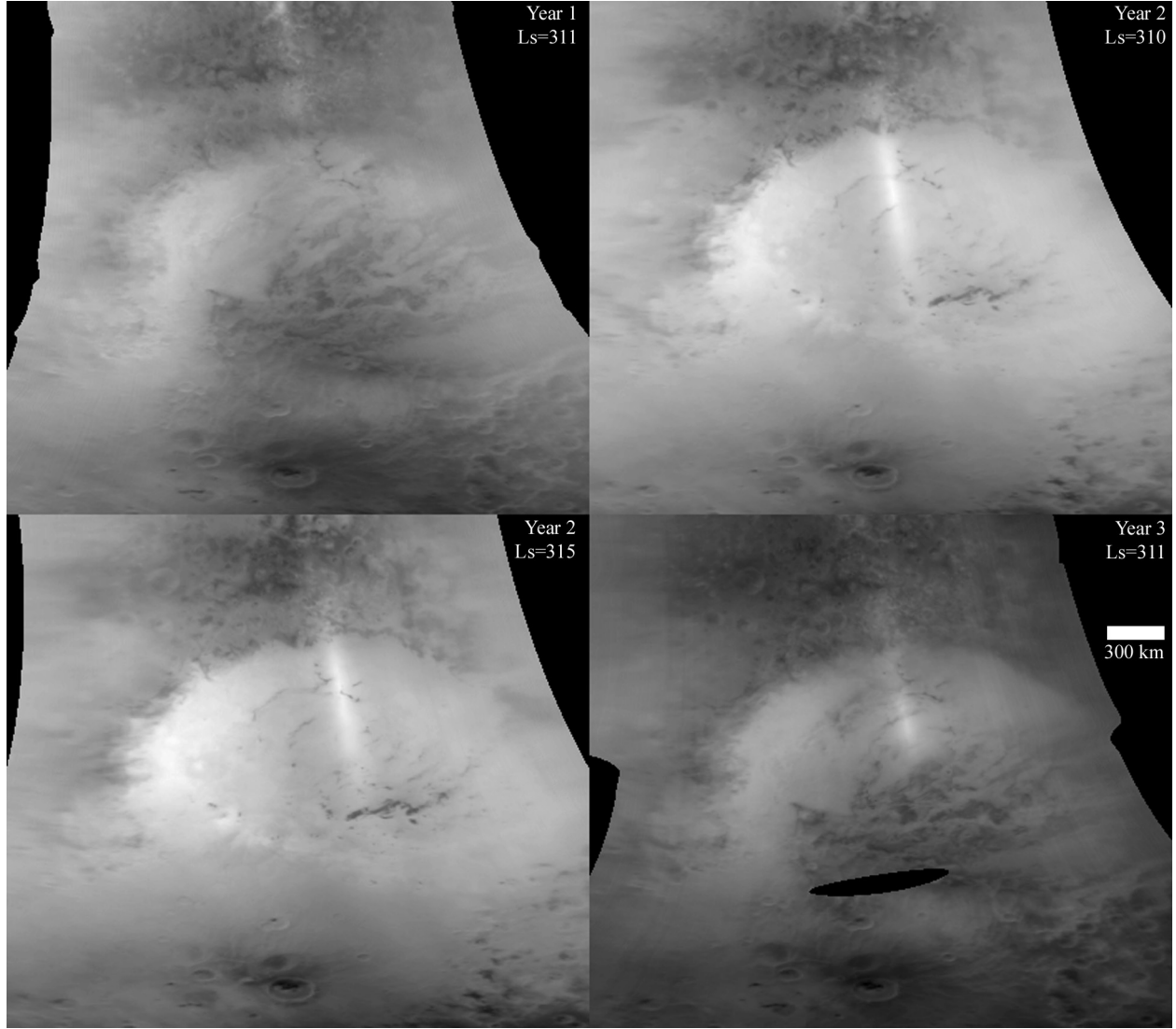
**Figure 10.** MOC WA DGM of Hellas during mid southern summer showing brightening after the 2001 global dust storm (second and third panels) compared to Year 1 (first panel), and then subsequent darkening by the same time in Year 3 (fourth panel).

with the albedo difference map of Figure 3b. A more detailed picture of this brightening is provided by MOC WA images within Hellas (Figure 11). These images clearly reveal the brightening of specific surfaces; the brightening is not an atmospheric effect which would reduce image detail and/or brighten the image en masse. The images suggest that Hellas indeed was blanketed with dust during the 2001 storm and was a net sink of dust.

[36] Figures 9 and 10 indicate that surfaces within Hellas returned to their pre-GDS albedo values by the southern summer of year 3. The temporal data in Figure 9 suggest that this transition occurred sometime during late southern winter. In fact, the MOC imagery and TES opacity data suggest that local cap edge dust storms develop during this period due to the thermal forcing of winds by the strong temperature gradient across the cap interface. The Hellas basin in particular appears hazy in images and has high dust opacities during this period. Although we cannot associate the albedo drop with a specific dust event or even state the

exact seasonal date(s) at which the dust in Hellas is removed due to the masking effect of the seasonal ice, we believe the data suggest that Hellas is cleared of the GDS dust by cap-edge winds during the following late southern winter and very early spring. These winds should be particularly strong in Hellas due to the combination of thermal contrast and slope [*Siili*, 1996; *Strausberg et al.*, 2005].

### 5.4. Hesperia

[37] Hesperia (17°S–31°S, 88°E–98°E) has a relatively flat albedo trend until the 2001 GDS (Figure 12). Small bumps near $L_s = 180°$ and 230° in year 1 are consistent with the timing of dust opacity peaks associated with seasonal cap edge dust storms and the "flushing" dust storm observed this year (Figure 1 and discussion thereof). Ice opacity appears to have negligible impact, with the modest ice opacity maximum in northern summer occurring at the time of an albedo minimum. The albedo following the decay of the GDS is higher than before the storm by about
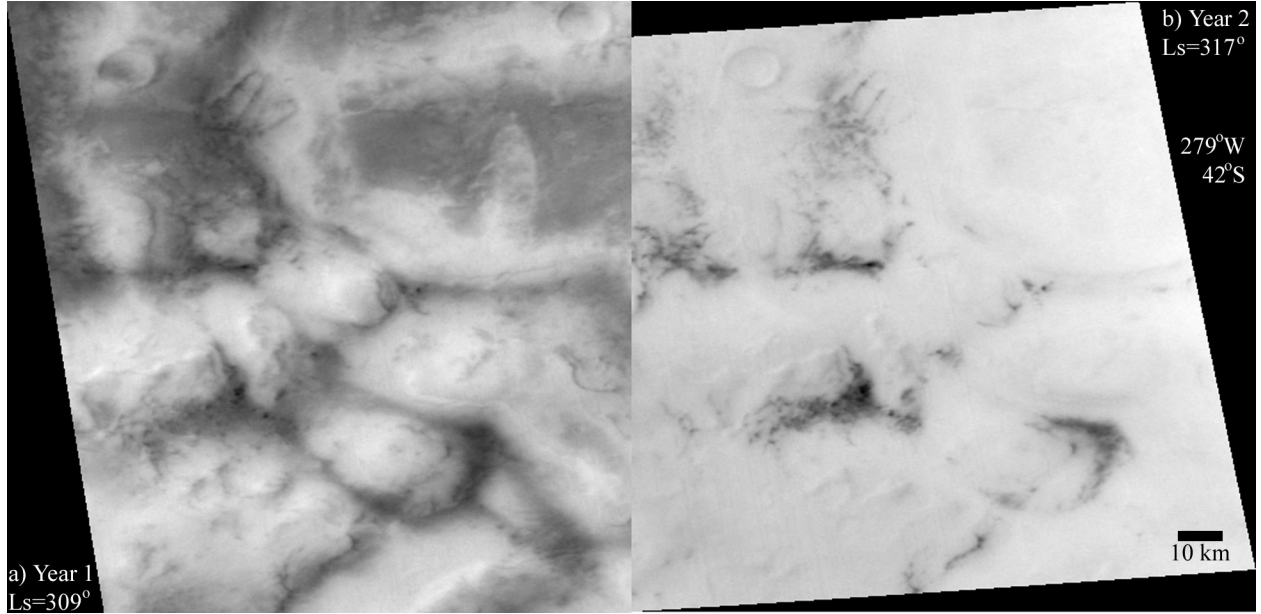
**Figure 11.** MOC WA images of Hellas near 42°S, 279°W showing brightening following the 2001 global dust storm from (a) Year 1, $L_s = 309°$ to (b) Year 2, $L_s = 317°$.
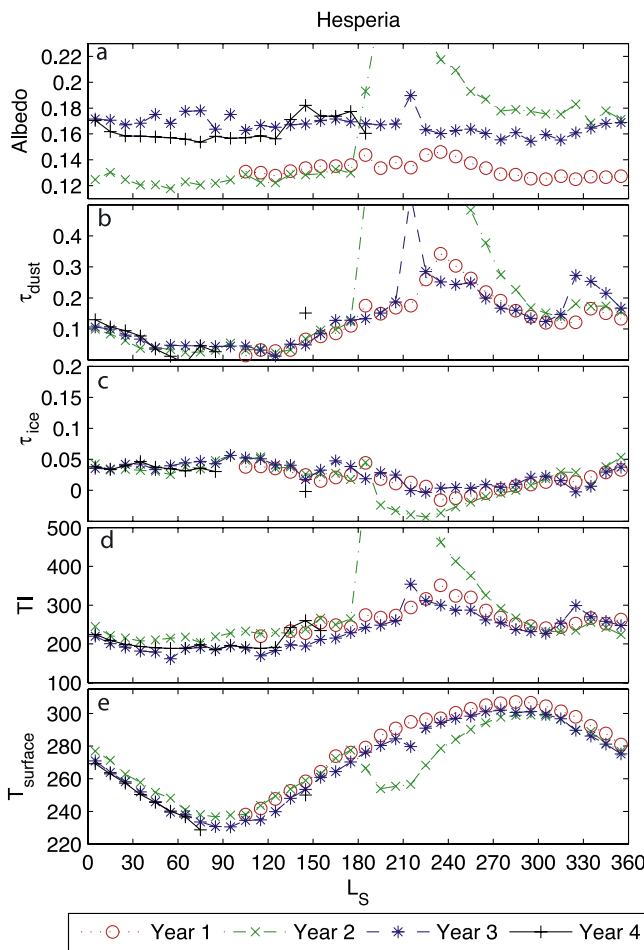


**Figure 12.** Similar to Figure 5 for our Hesperia region of interest (17°S–31°S, 88°E–98°E).

0.05–0.06 (or about a 40% increase) and remains near this higher value throughout years 3 and 4. A small decrease in albedo between $L_s = 210°$ and 315° in year 3 may be associated with dust activity evident in the dust opacity plot. Perhaps the $L_s = 210°$ dust storm resulted in dust removal, while the event at $L_s = 315°$ resulted in deposition.

### 5.5. Sirenum

[38] The albedo at Sirenum (39°S–53°S, 172°E–180°–166°W) follows a complex seasonal cycle (Figure 13). During southern spring and summer, the muted signatures of atmospheric opacity owing to dust storms are evident in years 1 and 3, while the GDS dominates year 2. The southern autumn and winter albedo trends have a pronounced set of variations that is repeated in the three years sampled. These variations are due to changes in atmospheric dust opacity as well as the presence of seasonal cap ice within the ROI.

[39] The changes in albedo resulting from dust redistribution can be separated from the seasonal trends. The 2001 GDS results in a ~0.04 increase in albedo for this relatively dark ROI, corresponding to a brightening of roughly 25%. However, following the retreat of the seasonal ice cap after $L_s = 180°$ in year 3 (one Mars year after the 2001 GDS), the albedo drops to a value intermediate between the prestorm and poststorm values. The darkening appears to occur during the seasonal ice cap retreat, as was also noted for Hellas, suggesting that thermal-contrast (sea-breeze) winds and related, small-scale cap-edge dust storms may be involved. It is tempting to infer a multiyear recovery in the albedo following the 2001 GDS, that is, a gradual darkening in years 3 and 4. However, we cannot rule out that dust redistribution by regional storms during this time period creates the appearance of such a trend.

### 5.6. Solis

[40] Solis, like Daedalia, has a historical record of albedo changes. *McKim* [1999] describes a number of changes that
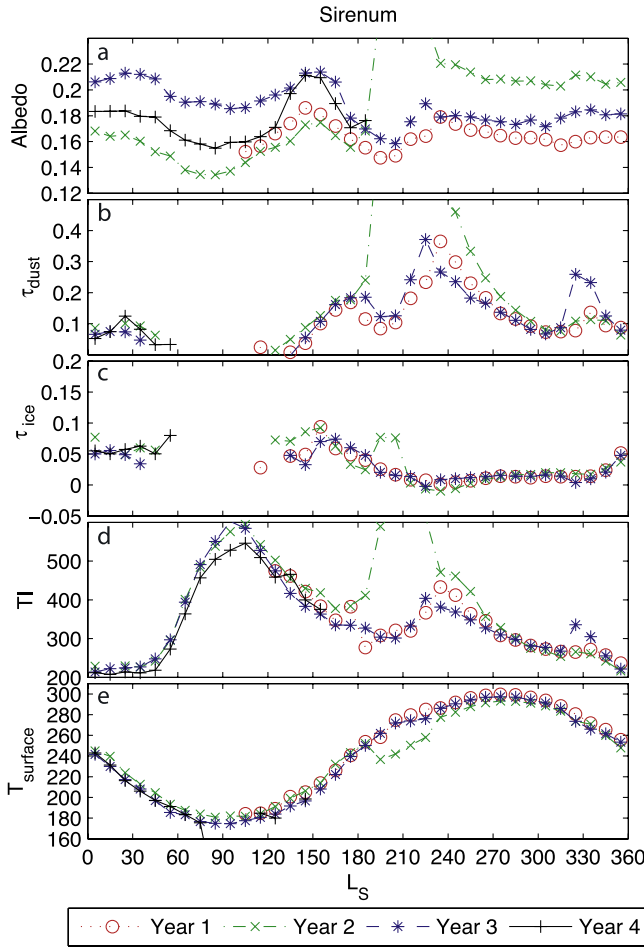
**Figure 13.** Similar to Figure 5 for our Sirenum region of interest (39°S–53°S, 172°E–180°–166°W).

Solis experienced in the 20th century. One example discussed by *Capen* [1976] is the brightening in the early 1970s. Solis was one of the focus areas of a study by *Lee* [1986], focusing on Viking data. *Lee* [1986] suggested that year-to-year changes in Solis may be due to differences in time of occurrence, severity, and longevity of dust storm activity.

[41] The section of Solis selected for the ROI (16°S–26°S, 67°W–80°W) shows little variation in albedo during the first complete year of observations (Figure 14). The southern spring and summer values are roughly 0.01 higher than the northern spring and summer values, consistent with the variation of atmospheric dust opacity. Between $L_s = 100°$ and $180°$ there is essentially no change between years 1 and 2, though both years vary in concert with the ice opacity. The impact of the 2001 GDS on Solis albedo is similar to that on Hellas, Hesperia, and Sirenum. There is a large jump in albedo that remains after the dust opacity decays. As with Sirenum (and perhaps more so here), the data imply a multiyear relaxation in the albedo trend toward pre-2001 values. Near $L_s = 300°$, the dust and ice opacities are essentially identical in the three years sampled. At this season, one can measure a decrease in the post-GDS albedo of 0.02 between years 2 and 3.

[42] Near $L_s = 315°$ in year 3 there is a sharp decrease in albedo, a jump in dust opacity, and image evidence of a relatively large dust storm. Figure 15 is a MOC WA DGM image showing this storm over the Solis ROI. The storm occurred just prior to the Mars Exploration Rover "Spirit" landing and caused some concern for entry, descent, and landing. As the dust opacity from this storm decayed, the albedo at Solis fell by 0.02 to a value of 0.17. It appears that while Solis was a net sink for dust during the 2001 global storm, it was a net source during the large storm of year 3.

### 5.7. Western Syrtis

[43] Syrtis Major is well known as a dark feature which often changes in appearance. The width of the dark region has historically cycled [e.g., *Sagan et al.*, 1973; *McKim*, 1999]. These changes have been attributed to a brightening caused by a global dust storm, followed by darkening caused by dust removal by aeolian processes [*Lee*, 1986; *Christensen*, 1988].

[44] The western Syrtis ROI (5°N–20°N, 59°E–68°E) brightens following the 2001 GDS (Figure 16). In the early northern spring, when atmospheric dust and ice opacities are low and similar in all years, the year 3 and year 4 albedos are about 0.04 (~20%) higher than in year 2 (prior to the global storm). The region containing our Syrtis ROIs (also
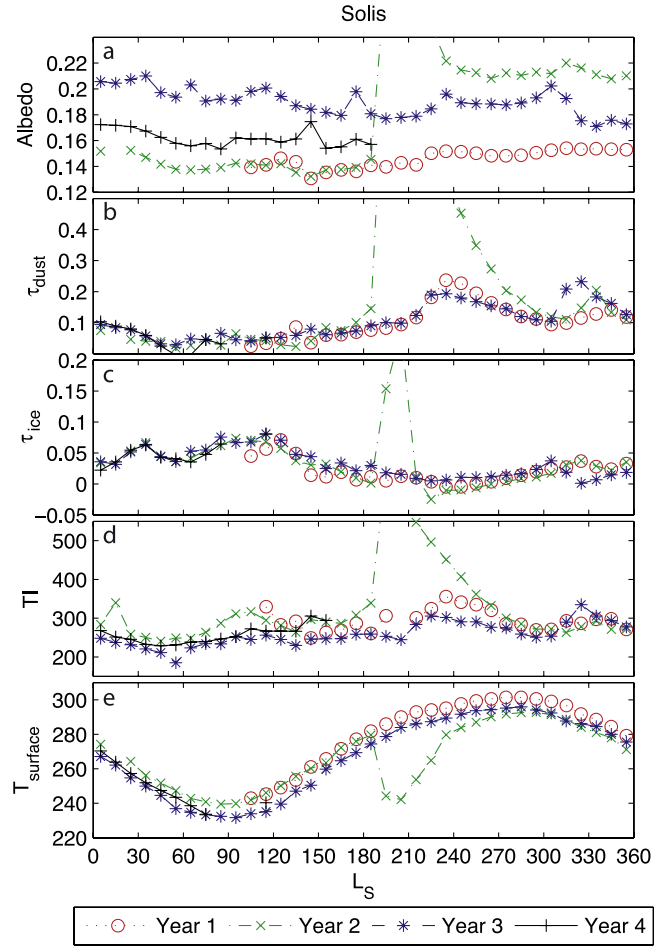


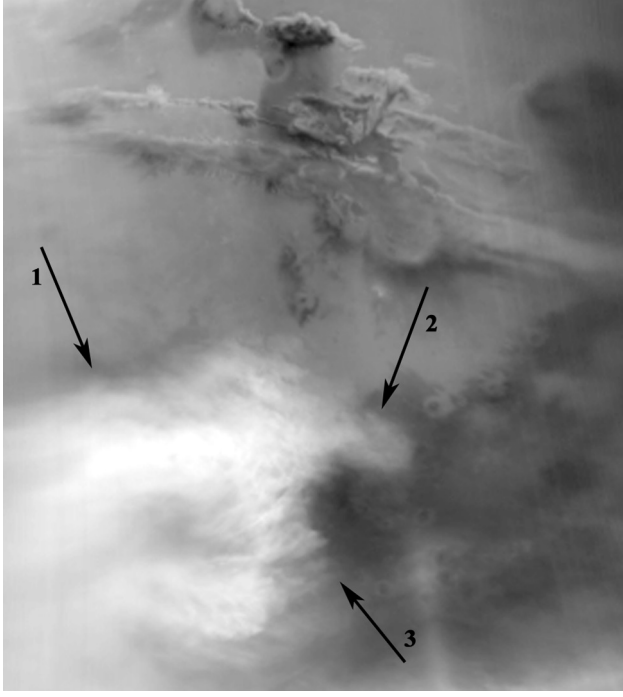**Figure 14.** Similar to Figure 5 for our Solis region of interest (16°S–26°S, 67°W–80°W).

**Figure 15.** MOC DGM showing the major regional storm near $L_s = 315°$ in Year 3 over the Solis area.

see section 5.8) received enhanced coverage by MOC, helping us to understand the nature of the albedo variations. Figure 17 shows sections of three MOC WA DGM red images. The western Syrtis ROI fills the middle left portion of each frame. Comparison of Figures 17a and 17b shows that the immediate effect of the GDS was to blanket many of the dark parts of Syrtis with brighter dust. Only a central, north-south segment remains somewhat dark. The newly brightened parts of Syrtis, especially in the central east, are somewhat less bright (probably less fully covered with dust) than the perennially bright surfaces further to the east in Isidis. Even immediately following the storm (Figure 17b), dust streaks can be seen in the lower central portion of the frame. By the time of the third frame, the extent of the brightening has lessened in the west, north, and east. In the north, several craters covered with dust in Figure 17b are partially cleared by the time of Figure 17c. And in the central left-hand side of the image, a large area of bright material seen in Figure 17b has been removed in Figure 17c. Across much of central and resurgently dark Syrtis, dusty wind streaks can be seen suggesting the role of large-scale winds in the dust removal. While most of these streaks appear newly formed in Figure 17c, and trend in a west-southwest–east-northeast (WSW-ENE) direction, a small portion of dust streaks can be seen in northern Syrtis in all three frames that trend in a direction at roughly 60° to these new streaks. Perhaps these were streaks formed during an earlier storm and wind clearing event, and remain as fossils through the turmoil of the 2001 storm and its aftermath. In any case, the image sequence shown in Figure 17 suggests a story of widespread net dust deposition as a result of the storm across much of Syrtis, followed by removal of material, apparently by large scale winds, during the course of the next several months.

[45] The box shown in Figure 17b corresponds to higher-resolution MOC WA red images collected before and after the 2001 storm. A selection of these images is shown in Figure 18. The first frame, taken just before the 2001 storm had expanded to global scale, shows a field of crater-related bright dust streaks. These streaks trend WSW-ENE and are superposed on lighter, apparently nontopographically related streaks running SW-NE. The effect of the 2001 GDS at this location is obvious. Figure 18b shows a nearly uniformly dust-covered scene. Crater rims can be seen due to shadowing, while the flat intervening surface is only lightly marked by dim streaking, trending in a range of directions from WNW-ESE to WSW-ENE. Between the end of the storm in late southern spring and around $L_s = 310°$ (Figures 18b–18e), the majority of the surface remains dust covered, but ongoing large scale wind action appears to be steadily working to clear dust. Note the steady increase of dark (erosional) streaking on the eastern edge of the region. These streaks resemble mesoscale linear streaks [*Thomas et al.*, 2003], rather than curvilinear dust devil tracks [*Malin and Edgett*, 2001; *Balme et al.*, 2003; *Fisher et al.*, 2005].

[46] Figures 18e–18g show a dramatic decrease in albedo as the sparse linear dark streaks expand and merge to leave only streaks of bright material in the protective lee of crater rims. What is surprising is that this transition takes place
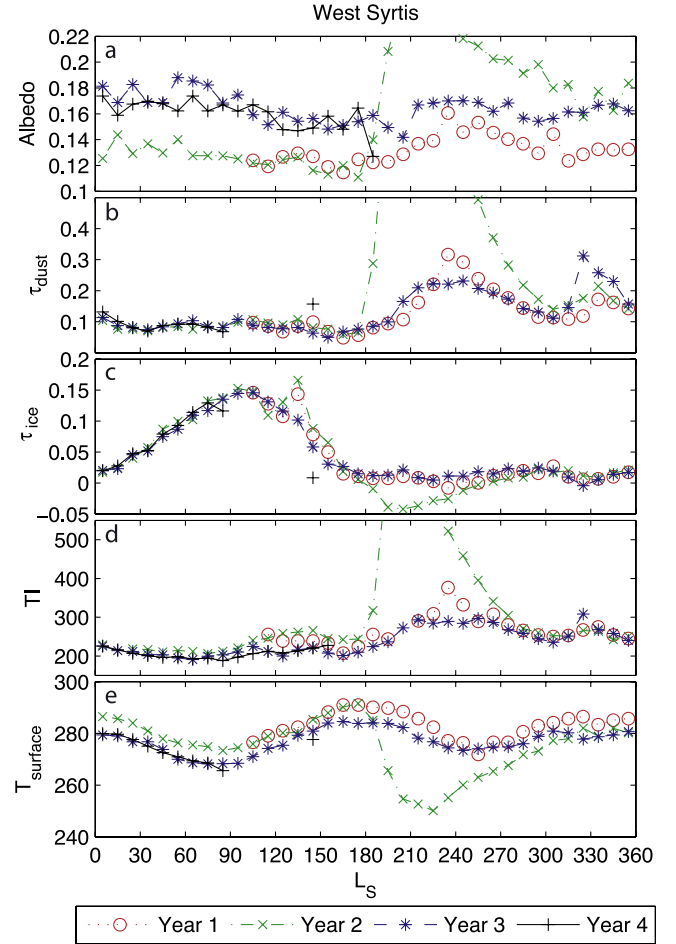


**Figure 16.** Similar to Figure 5 for the West Syrtis region of interest (5°N–20°N, 59°E–68°E).
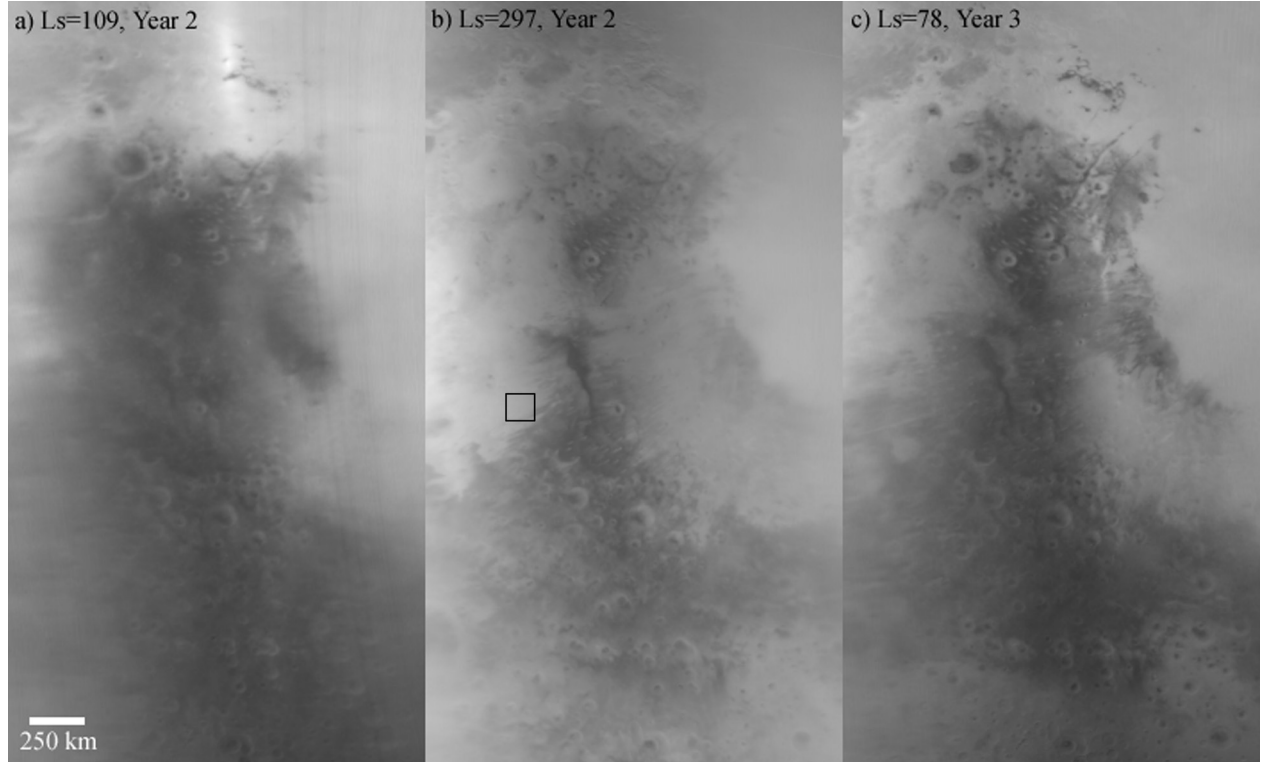
**Figure 17.** MOC WA DGM red images of Syrtis Major showing the brightening after the 2001 global dust storm (GDS) and subsequent darkening. Images are shown for (a) Year 2, $L_s = 109°$ (prior to 2001 GDS), (b) Year 2, $L_s = 297°$ (shortly after clearing of 2001 GDS), and (c) Year 3, $L_s = 78°$ (after 2001 GDS). The box in Figure 17b corresponds with the area shown in Figure 18.

gradually over about only one week (roughly $4-5°$ of $L_s$), and that this week is $\sim 50°$ of $L_s$ after the end of the GDS. The progression from 18e−18g shows substantial changes between each frame, suggesting that the wind event responsible for this removal was sustained over several days. The timing does not correspond with a significant dust storm, suggesting that the increase in surface wind stresses needed to lift the dust may not depend upon local feedback with lifted dust (i.e., some other process of wind intensification at this season may be involved). Figure 19 shows the more quantitative TES albedo and dust opacity history for the area shown in Figure 18. These data show that as the atmospheric dust opacity decays, albedo in the region decreases, but appears to be relaxing to a value near 0.2. However, at about $L_s = 315°$ there is a dramatic drop in albedo that has little correspondence with the dust opacity (though a slight rise in opacity at this time might be a signature of the dust being removed from the surface). After the drop, albedo remains steady at about 0.15, above the prestorm value of about 0.11. The albedo data clearly confirm a dramatic drop in albedo at $L_s = 315°$, in good agreement with the images in Figure 18.

[47] The bright streaks apparent after half a year of poststorm dust removal align well with those evident before the storm. Furthermore, the bright streaks appear to form through protection of previously deposited material rather than preferential deposition of dust in crater lees. The former issue supports the idea that dust removal following large dust storms occurs at similar seasonal dates in different years (i.e., by similar seasonal wind patterns). The high temporal resolution afforded by the MOC imagery yields some insight into the formation mechanism for the bright streaks. However, the imaging data cannot address whether the bright streaks are older deposits of bright material that simply become buried by dust from the GDS and subsequently exhumed.

### 5.8. Northern Syrtis

[48] Northern Syrtis (22°N–27°N, 67°E–79°E) is one of the minority of locations that was a net source of dust to the 2001 GDS (surface dust coverage was reduced by storm). The spatially averaged albedo reduction was roughly 0.02–0.03 or about 12% (Figure 20). However, the darkened region is small and irregularly shaped, surrounded by areas of brightening (Figure 3). Some surfaces darkened by as much as 0.05. The thermal inertia shows no year-to-year changes, suggesting that the variations in dust cover thickness were less than centimeter-scale. The MOC WA images of northern Syrtis show how the albedo change there corresponds with changes in the appearance of the Syrtis region (Figure 17). Specifically, the area to the ENE of the larger crater in northwestern Syrtis (an arrow was not added so as not to obscure features in the image) shows a net loss of dust between Figures 17a and 17c. The bright dust cover has retreated to the north and east as a result of the storm, contrary to the evolution of much of Syrtis. In fact, Figures 17 and 20 show that this darkening occurred immediately following the storm, synchronous with the wind events that cleared much of central and southern Syrtis (section 5.7). Figure 20 shows that the year 2 albedo remained very
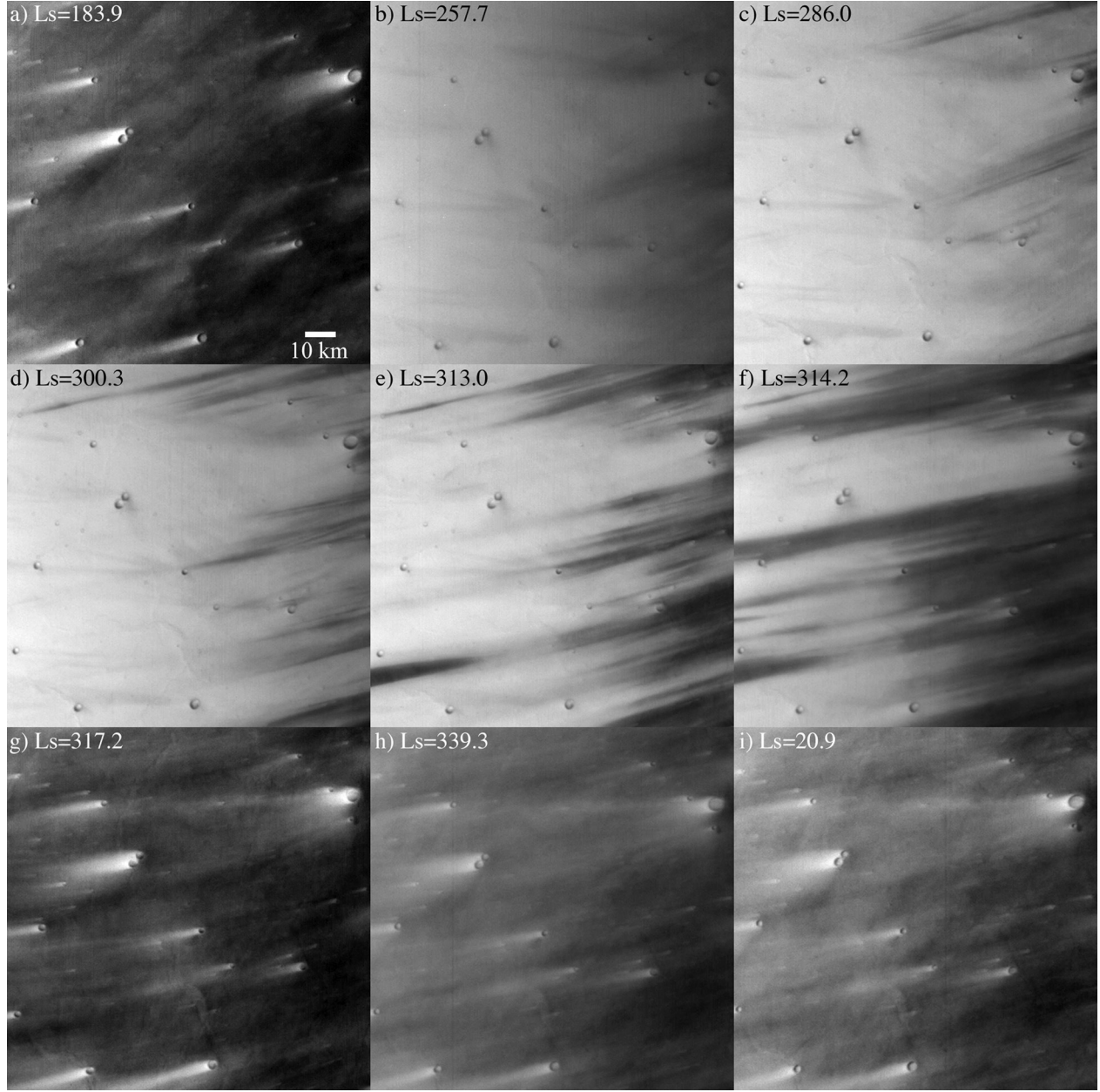
**Figure 18.** Series of MOC WA images of the portion of Syrtis Major indicated in Figure 17b (near 5°N, 64°E). The images show (a) a dark surface prior to the 2001 GDS, (b−d) a bright surface following the 2001 GDS, (e−g) rapid clearing of the deposited dust, and (h and i) the long-term preservation of the resulting surface condition.

similar to that of year 1 at $L_s = 300°$ (a relatively clear period). It is only following $L_s = 300-330°$ that the albedo falls to the values of year 3. This timing is supported by the images that show the Northern Syrtis ROI to be nearly completely dust covered at $L_s = 297°$ in year 2. But by $L_s = 78°$ in year 3, the darkened area seen in Figure 3 has cleared.

## 5.9. Western Arcadia

[49] The western Arcadia ROI (34°N−43°N, 172°E−180°E) bounds a distinctive low-albedo feature whose shape changed during the MGS mission. The combination of TES albedo and frequent MOC WA DGM image coverage

allows us to identify the specific event that led to this change. The albedo record contains a great deal of intra-seasonal variability in southern spring and summer, most of which is directly ascribable to atmospheric dust opacity (Figure 21). During the first three years, the northern summer albedos are similar (except for the very first data point, which we believe is spurious on the basis of comparison with images). The major change in surface dust suggested by the data occurs between the end of summer in year 3 and the start of spring in year 4, when the albedo increases by about 0.02−0.03 or roughly 10%.

[50] Figure 22 shows MOC WA DGM red images for five seasonal dates in year 3 and one in year 4. The first frame
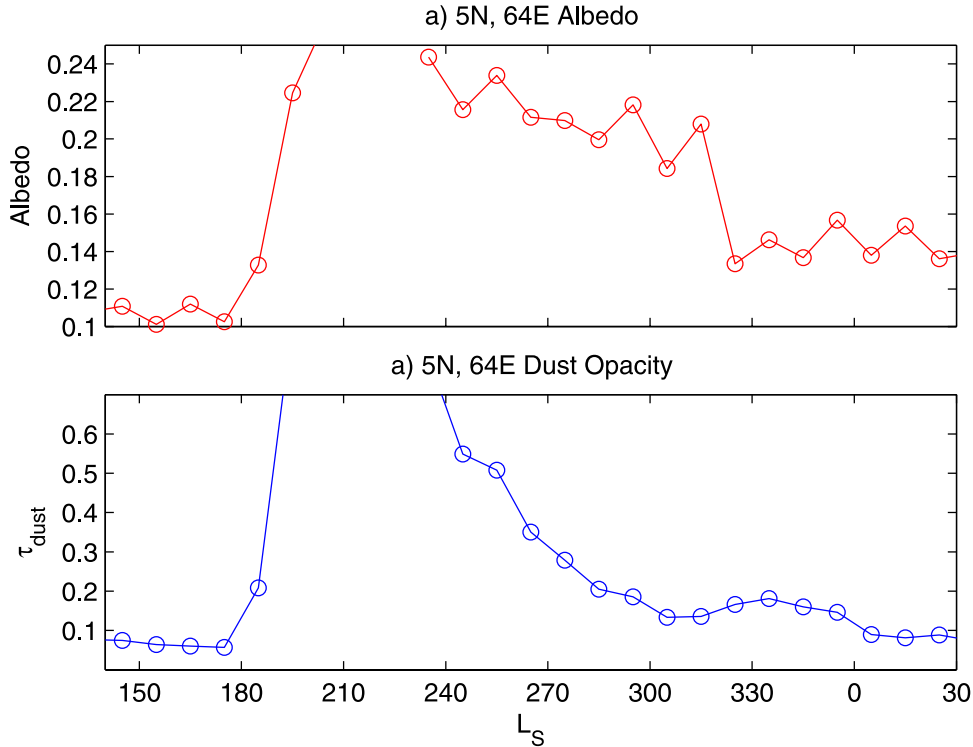
**Figure 19.** TES albedo and dust infrared opacity record of the area of Syrtis Major in 3°N–7°N, 62°E–66°E (approximately the area shown in Figure 18) from Year 2, $L_s = 120°$ to Year 3, $L_s = 30°$.

shows the low-albedo feature that defines this ROI, an oval area roughly 250–300 km across, with a tail of dark material extending to the north and west. Figure 22a shows the feature as it appeared from the start of the MGS until the late summer of year 3. By mid autumn (Figure 22b) the feature appears largely unchanged, though it is somewhat harder to observe due to the low solar incidence angle and the development of high-latitude water ice clouds. However, by the time of Figures 22e and 22f, bright material (taken to be dust) has been deposited across the center of the feature, separating the oval portion of the feature from the remnants of the tail. This brightening corresponds with the increase in TES albedo in Figure 21.

[51] A dust cloud was observed to develop over the western Arcadia ROI and much of the nearby area after $L_s = 211°$, as shown for $L_s = 213°$ in Figure 22c. Given the dramatic nature of the Figure 22c image, it is tempting to immediately ascribe the brightening to this storm. The tendency for storms to occur near bright-dark boundaries in the northern hemisphere as observed in MOC images has also been discussed by *Cantor et al.* [2001]. Figure 21 shows that there were, in fact, two major dust storms that affected the ROI (as well as much of the planet as shown by Figure 1) in year 3, one after $L_s = 200°–210°$ and one after $L_s = 300°$. However, images from the relatively clear period between $L_s = 270°$ and $L_s = 300°$ (Figures 22d and 22e) show that the brightening had occurred before the second storm.

### 5.10.  Eastern Arcadia

[52] The eastern Arcadia ROI encompasses a low-albedo feature within Arcadia (Figure 3), chosen in order to study the nature of change in surface markings with MOC WA DGM data. The feature in eastern Arcadia is a linear, east-west running dark region in the earliest mapping images collected by MOC (Figure 23a shows the feature at $L_s = 305°$ in year 1, appearing as it did from the start of mapping). The feature had a length of roughly 300 km, a north-south width of ~30 km, and exhibited increased width (to ~50 km) to the north and toward the east of center. In the east, the low-albedo marking was crossed by a number of thin, bright lineations. By $L_s = 350°$ in year 1, the right-hand portion of the feature, from the region of increased width and eastward, had been covered in bright dust (compare Figure 23a and 23h, specifically the feature indicated by the topmost arrow in Figure 23a). These images constrain the timing of the brightening to between $L_s = 329°$ (Figure 23c) and $L_s = 338.3°$ (Figure 23g), a period of a little more than two weeks.

[53] Figures 23b and 23d–23f show local/regional storm events that can be associated with the low-albedo feature in year 1. Clearly some persistent trigger for dust storm activity existed at this location and time since the small storm evident in Figure 23b completely decayed before the start of the much more extensive activity shown in Figures 23d–23f. In all cases, the dust clouds do not extend greatly beyond the environs of the low-albedo feature, and are isolated such that the dust most likely was lifted from the bright material surrounding the low-albedo feature. Indeed, it is possible to convince oneself that plumes of lifting can be seen on the fringes of the storm, especially on the southwestern edge of the cloud in Figure 23e. In any case, in Figures 23d and 23e, the atmospheric dust is seen to skirt the southern boundary of the low-albedo feature, and then
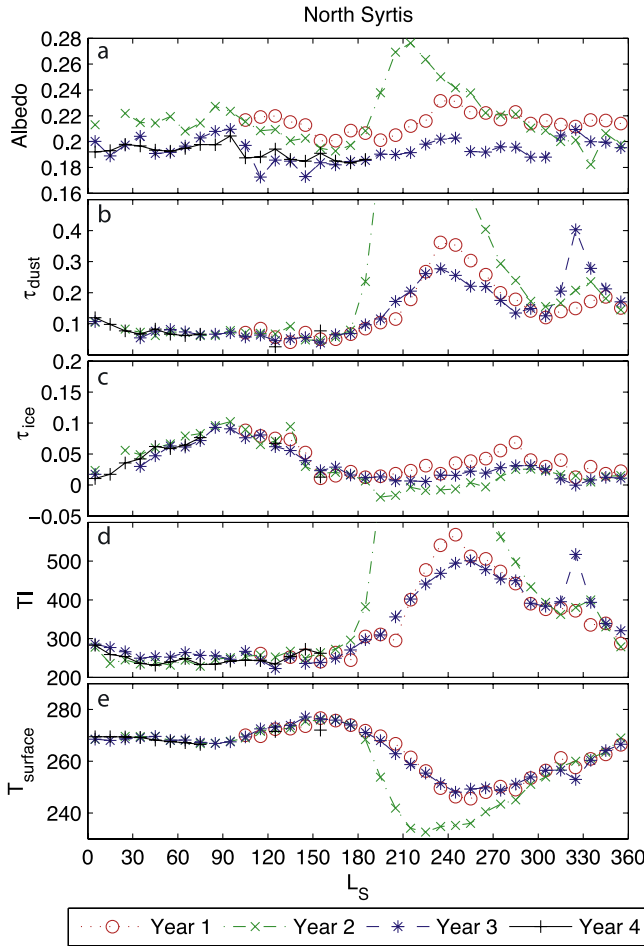
**Figure 20.** Similar to Figure 5 for our North Syrtis region of interest (22°N–27°N, 67°E–79°E).

cut north across the eastern portion of the feature, to the east of the centerline of the dark feature's hump. This is the area of formerly dark surface that is dramatically brightened following the storm, and has arguably already been brightened by the time of Figure 23f.

[54] In addition to the brightening of the eastern portion of the low-albedo feature, the dust events of $\sim L_s = 330°–337°$ wrought more subtle changes on the surface. The western tip of the low-albedo feature in Figure 23a (leftmost arrow) was blunted by the storm. Dark streaks (mesoscale linear streaks [*Thomas et al.*, 2003]) indicative of a previous period of wind erosion (lowermost arrow in Figure 23a and evident in Figures 23b and 23c) were eliminated by the storm. These streaks appear to have been erased by the removal of the bright material into which they were cut, rather than by burial. A new high-albedo (high dust cover) feature generated by the storm is indicated by the arrow in Figure 23h. This bright tail of material trends to the north and east and merges with the generally bright material observed to cover the formerly dark eastern portion of the low-albedo feature and immediate environs.

[55] The changes in the eastern and western Arcadia regions during the MGS mission appear to have been the result of very rapid redistribution of dust by dust storm events. In the case of eastern Arcadia, the dust storm development appears to be related to the presence of the

low-albedo region, because the extent of the dust cloud is of the same order as the low-albedo feature and very closely superposed. In any case, these two regions suggest that large, "catastrophic" events are more important for changing (brightening) recognizable dark surface markings on the planet than the steady action of lower intensity processes. This is also supported by the observations in Syrtis. Depending upon whether one considers one season's worth of seasonal cap-edge storm activity steady or catastrophic, the dust resurfacing trends at Hellas and Sirenum are also consistent with this conclusion.

## 6. Dust Redistribution Between Viking and MGS

[56] The combination of albedo and thermal data from the Viking and MGS orbiters provides the opportunity to assess changes and variability in surface dust distribution over a Martian decade. Some caution is warranted, however, by the large time gap between the missions and by differences in how the data sets were collected. The time gap allows us to observe the cumulative effects of processes ongoing for a period exceeding twice the length of the MGS mapping mission. But it does not allow the nature of those processes to be inferred (specifically through the timescale over which they occur), as do the frequent MOC observations described in section 5. The differences in data collection are two-fold. The MGS is nadir-pointed and collects data continuously from a low, circular, sun-synchronous orbit, yielding nearly uniform (and low) emission angles for albedo measurements. The Viking orbiters were in elliptical and variable orbits and viewed the surface at a variety of emission angles. The nearly complete global coverage provided by MOC WA every Martian day is contrasted with the targeted images of Viking. The global mosaics assembled from Viking images are far from instantaneous "snapshots."

[57] The changes in albedo inferred from Viking and MGS imagery are described in detail by *Geissler* [2005]. Two major types of changes are noted: a widespread darkening of the southern mid and high latitudes, and changes in the shape and extent of low-albedo regions in the northern tropics to high latitudes. We reexamine the
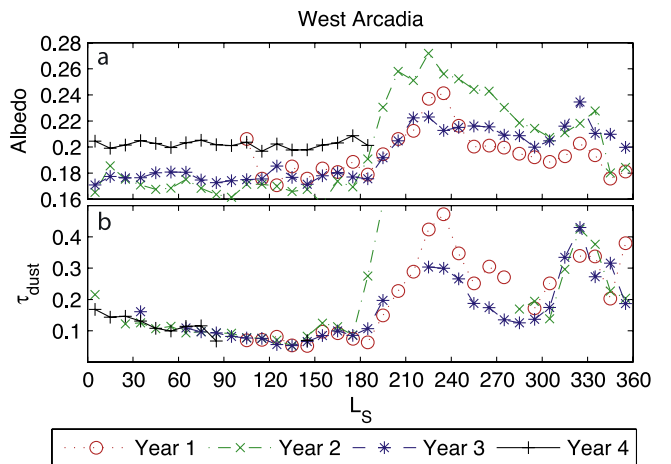


**Figure 21.** Similar to Figure 5 for our West Arcadia region of interest (34°N–43°N, 172°E–180°E), but showing only albedo and dust infrared opacity.
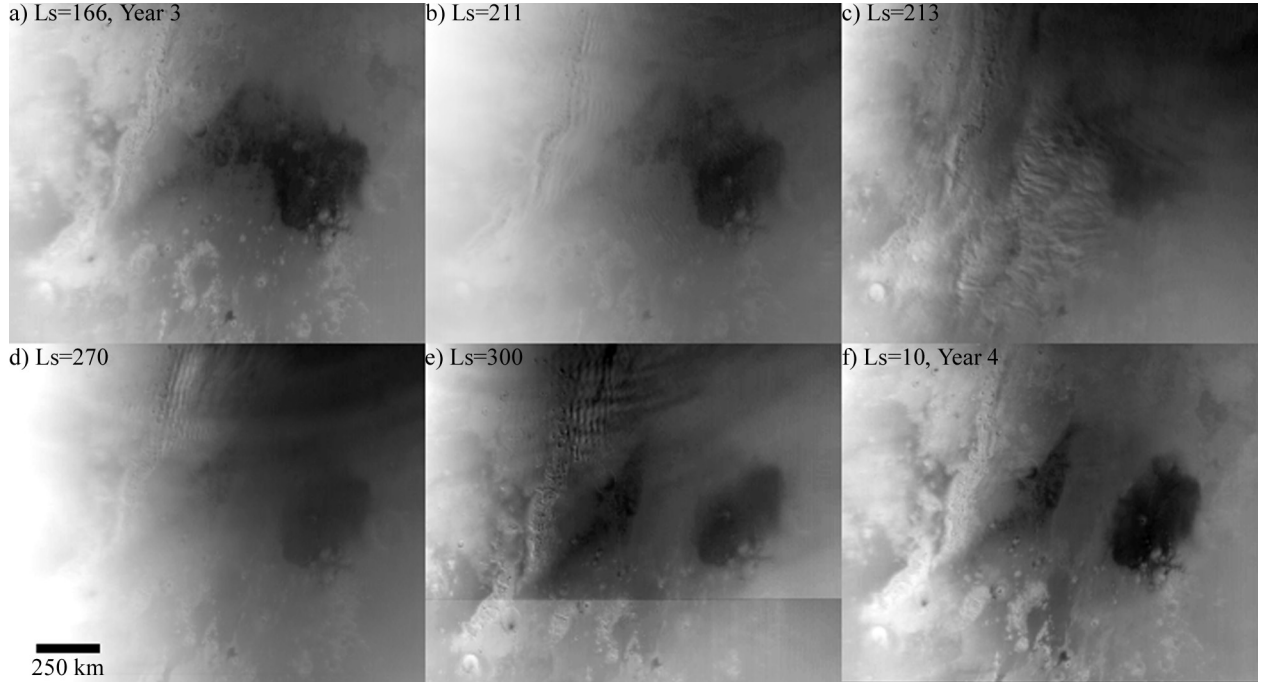
**Figure 22.** Series of MOC WA DGM red images of the West Arcadia region of interest showing the change in the surface caused by the first major regional dust storm of Year 3.

darkening of the southern hemisphere in order to understand how the irregular sampling of Mars over the past decades impacts our ability to understand the nature of the processes that have redistributed surface dust, especially our ability to assign timescales to changes. We also use new analyses of albedo and imaging data to test some of the hypotheses developed by *Geissler* [2005] to explain several regional albedo changes. Specifically, we ask whether dust devils play a significant role in the modification of low-albedo regions.

### 6.1. Southern Hemisphere

[58] Figure 2 from *Geissler* [2005] (similar to our Figure 24) shows a dramatic change in the albedo of much

of the southern mid and high latitudes between the acquisition of the Viking Mars Digital Image Model (MDIM) [*McEwen and Soderblom*, 1993; *McEwen et al.*, 1993] and the composite MGS "cloud-free" global map [*Geissler*, 2005]. At face value, it appears that large areas of the surface that were covered by dust during the Viking era were substantially freer of dust during the MGS era. Any widespread, secular evolution in albedo would obviously be important for our understanding of climate dynamics and the geologic evolution of the surface layer. However, how sure are we of the degree to which these two maps are truly representative of their respective eras? Indeed, after reviewing the Viking and MGS era imaging and albedo observa-
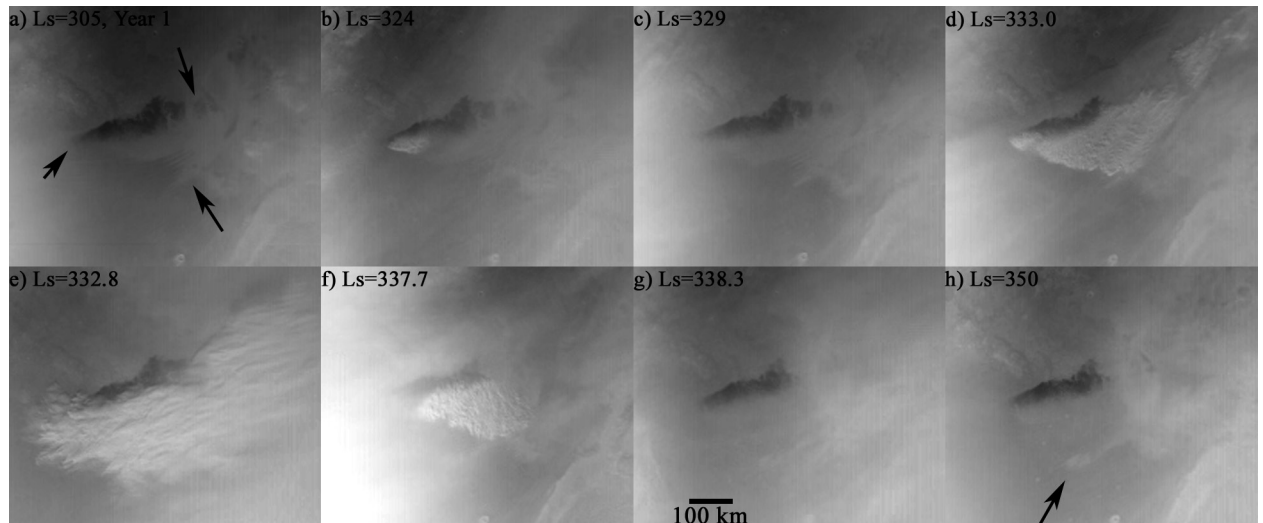


**Figure 23.** Time series of MOC WA DGM images of the East Arcadia region of interest during Year 1, from $L_s = 305°$ to $L_s = 350°$.
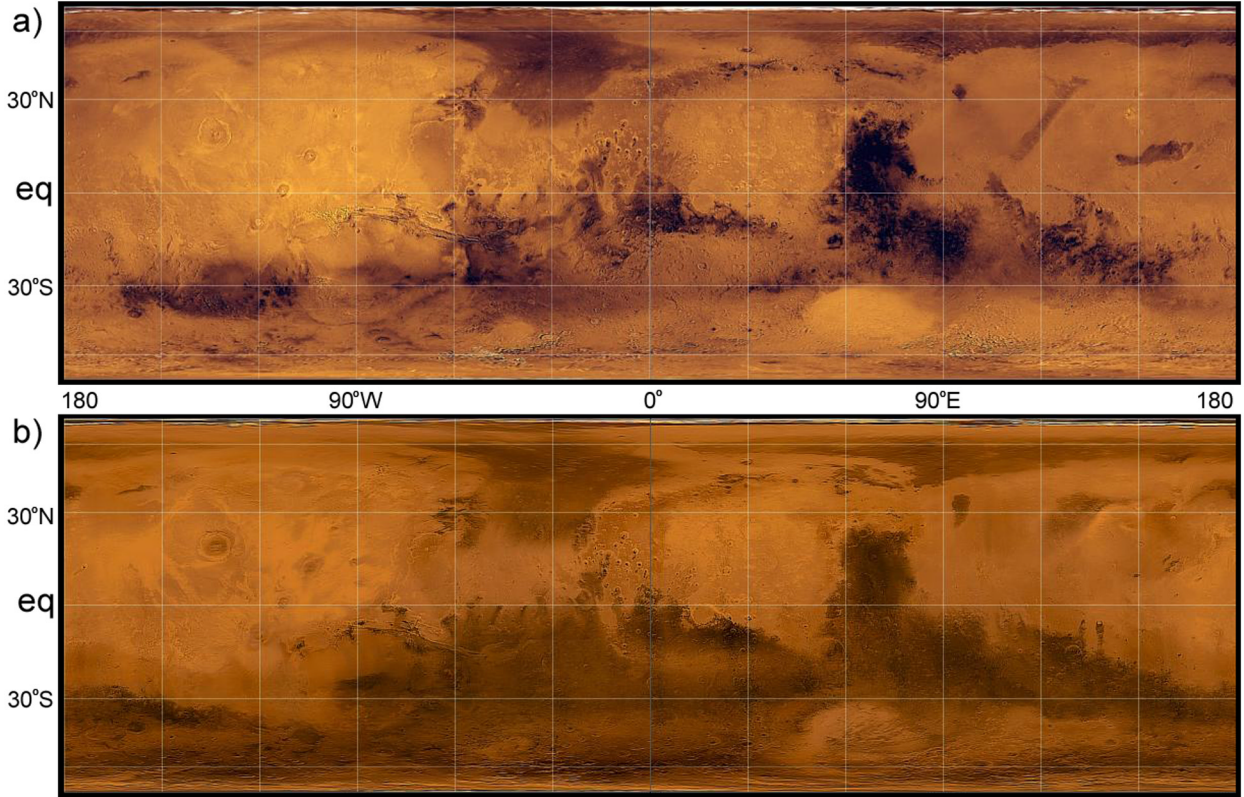
**Figure 24.** Comparison of Viking and MGS global mosaics. (a) Viking MDIM created by *McEwen et al.* [1993] using images taken after the 1977 global dust storms. (b) Cloud-free mosaic of MGS images taken before the 2001 global dust storm, modified from *Geissler* [2005, Figure 2].

tions, we find that Figure 24 contrasts an extreme case of widespread dust cover following a major dust storm (Viking MDIM) with a highly "cleaned" surface prior to the 2001 storm (MGS mosaic). If the imaging data for the Viking era in Figure 24 had been acquired before the 1977 storms, the IRTM data suggests that a darker surface would have been noted in the south. Similarly, MOC imaging and TES albedo observations acquired just after the 2001 storm show bright southern mid and high latitudes, comparable to or brighter than observed at the same seasonal date in 1977. These observations suggest that that the comparison in Figure 24 yields important information about the aftermath of large storms (and specifically about the role of southern seasonal cap edge storms in cleaning dust deposited in the mid and high southern latitudes, see below). In a more general sense, they show that widespread albedo changes such as the darkening/brightening of the southern hemisphere can occur rapidly, on a timescale even shorter than a season. Accordingly, they reveal the difficulty in deciphering decadal-scale, secular evolution in the sparsely sampled Viking-MGS record. The above summarizes our major finding in this section; below we provide details of our analysis.

[59] Figure 25 is a timeline of the major dust storms and data collection intervals during both the Viking and MGS eras. The majority of the Viking MDIM data come from a year that included two GDS's (1977a and b), and follows a Martian year that also exhibited a major storm (it is interesting to note that although this 1975 storm does not

appear in the list compiled by *Martin and Zurek* [1993], it was extensively observed by amateur astronomers, as described by *McKim* [1999]). Global storm activity occurred in each of the southern summers from 1971 to 1977 [*McKim*, 1999]. The Viking MDIM images of the southern mid and high latitudes used to make Figure 24 were acquired during late southern summer immediately following the 1977b GDS (images are from $L_s = 297° - 342°$, and mostly after $L_s = 320°$) [*McEwen and Soderblom*, 1993]. By contrast, neither the year preceding the start of the MGS mapping mission nor the first MGS mapping year contained a GDS [*Smith et al.*, 2000; *Liu et al.*, 2003; *Smith*, 2004]. It is from this pre-2001 GDS period that the MGS image map data were collected.

[60] A more complete and quantitative picture of the variation of albedo within the Viking mission can be obtained by examining maps of binned IRTM albedo data from restricted ranges of $L_s$. Figure 26 shows such maps for early southern spring, just prior to the 1977a storm; for late southern spring, just after the end of the 1977a storm and just prior to the 1977b storm; and, for late southern summer/early southern autumn after the 1977b storm (corresponding to the date of acquisition of the MDIM images). Data from northern summer are not useful because of the low illumination at the southern high latitudes. A major difference between the Viking MDIM and the MGS mosaic in Figure 24 is the uniformity of bright surface across the high southern latitudes (south of 30°S–45°S, depending on longitude) in the former, while the latter is
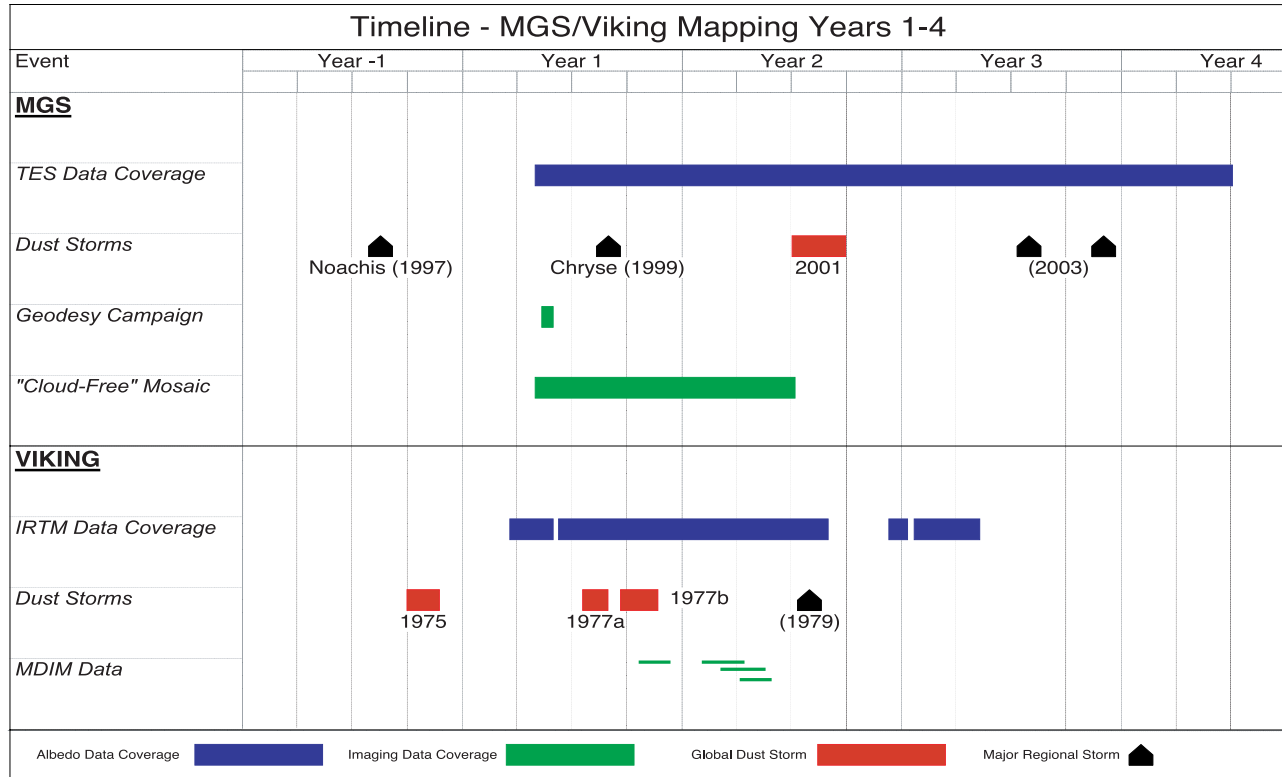
**Figure 25.** Timeline for Mars indicating the periods of albedo data collection, occurrence of major dust storms, and the periods of collection of the imaging data making up the Viking MDIM and MGS geodesy and cloud-free global images.

characterized by relatively dark mid and high southern latitudes, apart from a bright spur extending and thinning to the east from Hellas to somewhere between 180° and 120°W. However, the early southern spring IRTM data (in particular the $L_s = 200°–210°$ data) show the southern midlatitude and high-latitude spatial pattern to be more reminiscent of the MGS mosaic than the Viking MDIM insofar as the bright areas that are not obviously the seasonal cap edge (very bright measurements along the southern edge of the data) form a bright spur extending to the east from Hellas. A distinct dark surface can be seen to the south of this spur, separating it from the seasonal cap edge. In the western hemisphere, the southern midlatitude and high-latitude surface is relatively dark all the way from the southern edge of the Tharsis high-albedo region (15°S–30°S) to the fringe of the southern seasonal ice cap (at roughly 50°S). Figure 26 shows that it is only following the 1977a storm, and especially after the 1977b storm, that the bright region extending from Hellas is seen to encircle the planet and extend continuously to the edge of data coverage in the south. Indeed, while much of this extension of the bright region occurs in the eastern hemisphere during the 1977a storm, the consolidation and development of continuous coverage in the western hemisphere results largely from the 1977b storm (Figure 26). Therefore a significant change in the brightness of the southern hemisphere occurred within the Viking observation period.

[61] The TES data collected for similar seasonal ranges and from years before and after the 2001 GDS are shown in Figure 26. It can be seen from these figures as well as from Figure 24 that aside from the zonal brightness of the southern mid and high latitudes in the poststorm (1977a and b) Viking data, another major difference in the albedo pattern is in the shape of the bright-dark boundary on the southern edge of Tharsis between about 60°W and 135°W. The Viking data (pre- and post-1977 storms) show a border that trends consistently north-east across this longitude range, while the pre-2001 storm MGS data show a major bright "peninsula" extending to the southeast at roughly 100°W. This is the bright material in Daedalia Planum that provides the dominant net source of material for the 2001 storm and is thus removed by the 2001 storm (see section 5.1). Indeed, data collected after late southern spring of 2001 show a southern Tharsis albedo boundary that is in quite good agreement with that observed by Viking.

[62] The similarities and differences between the Viking and MGS data before and after the 2001 storm can be seen more clearly in Figure 27, which shows the albedo difference between the IRTM and TES data for $L_s = 340°–350°$ and $L_s = 250°–260°$. MGS mapping years 1 and 2 are shown for both periods. The removal of material from the Daedalia Planum "peninsula" following the 2001 storm is apparent in both seasonal windows (compare the year 1 and year 2 differences from Viking). The 2001 storm results in a substantial reduction of the difference between Viking and MGS albedos over the Tharsis plateau, and specifically over Daedalia. Indeed, this storm appears to bring the surface dust distribution observed by MGS much closer to the state observed by Viking. For the late southern spring comparisons ($L_s = 250°–260°$), the 2001 storm had a much
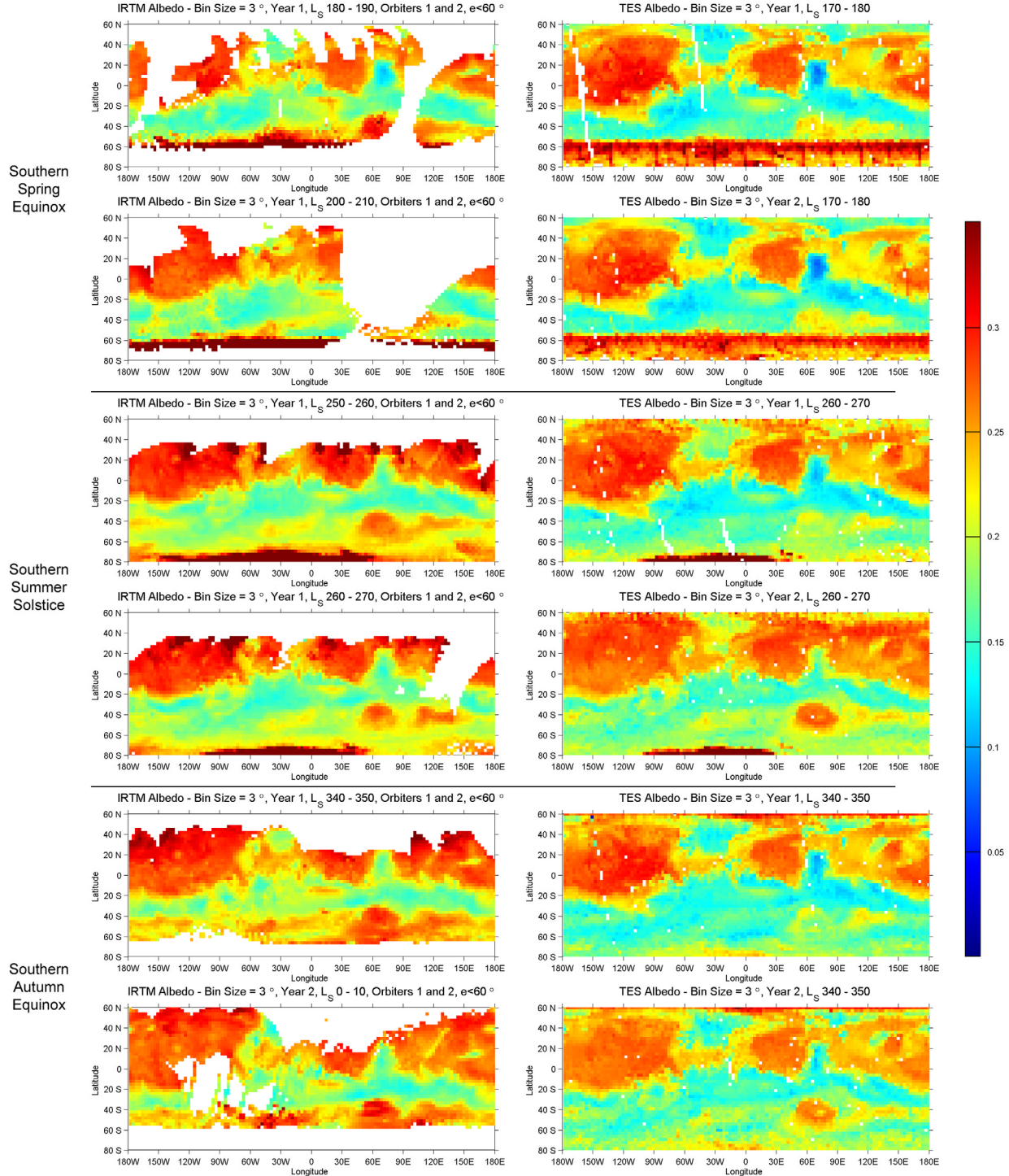
**Figure 26.** Comparison of albedo data from Viking IRTM and MGS TES for early southern spring, just prior to the 1977a storm; for late southern spring, just after the end of the 1977a storm and just prior to the 1977b storm; and for late southern summer/early southern autumn after the 1977b storm. All data were binned by 3° of latitude and 3° of longitude.

stronger brightening effect on much of the surface than the smaller 1977a storm observed by IRTM. The Hellas basin and much of the surface to the east, especially near the 30°S zone, were greatly brightened by the 2001 storm relative to the surface observed by IRTM. Indeed, for late southern spring, apart from the very high southern latitudes, the MGS

mapping year 2 surface appears brighter than the Viking year 1 surface. However, the effect of the 1977b storm in brightening the surface observed by IRTM combined with the "cleaning" effects of winds in the southern summer following the 2001 storm means that by late southern summer, the Viking observations have brightened substan-

**Figure 27.** Difference between IRTM Year 1 and TES albedo measurements for $L_s = 340° - 350°$ and $L_s = 250° - 260°$ for both TES Year 1 and TES Year 2. Blue indicates areas that were brighter in the IRTM data, while red indicates areas that were brighter in TES data. An emission angle limit of $60°$ was used to constrain the IRTM data. All data were binned by $3°$ of latitude and $3°$ of longitude.

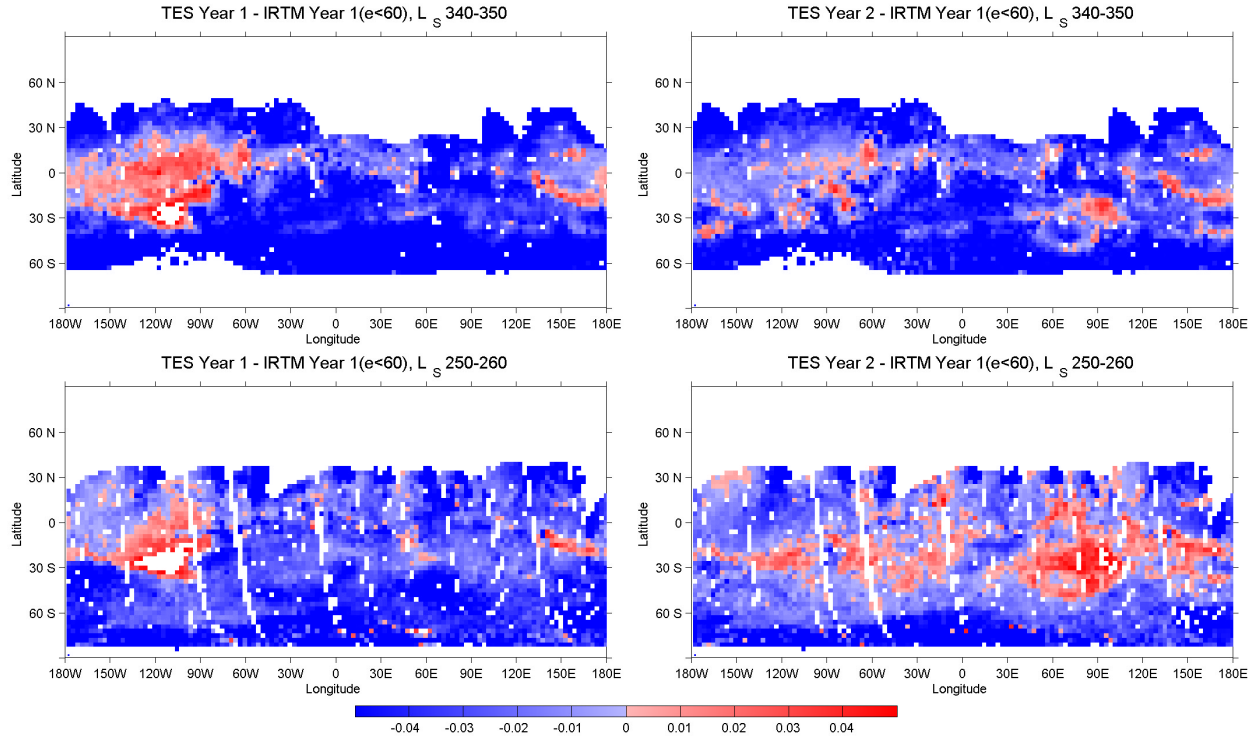tially relative to MGS (i.e., note the "bluing" of the "TES Year 2" difference plots from southern spring to southern summer).

[63] The timing of the 2001 and 1977b storms in particular should be noted. The origin of the 2001 storm before $L_s = 180°$ and its demise following $L_s = 215°$ means that dust laid down by this storm in the southern mid and high latitudes was on top of the seasonal ice cap. We have shown that the trend of albedo at locations along the seasonal cap edge indicates that the retreat of the seasonal cap (and presumably, the associated strong thermal-contrast circulations) is a powerful process for "cleaning" the surface of air fall dust following the 2001 storm (see section 5.5). On the other hand, the 1977b storm began only after $L_s = 270°$, when the southern high latitudes were already largely free of seasonal ice. As a result, the seasonal ice cap edge and its associated wind systems did not have a chance to modify the surface dust deposited by the 1977b storm (it presumably did so the following year, but IRTM did not collect data to see it). In this sense, the 1977b event was the "perfect storm" for maximal evidence of surface dust deposition in the southern mid and high latitudes.

[64] Comparison of albedo maps show that some areas of the surface are brighter in the MGS record than in the Viking record and vise-versa. In general, the Viking observations show a brighter surface, with the comparison least favorable to Viking when assessed against the southern summer solstice data from MGS mapping year 2. The second question introduced at the start of this subsection was, to what degree do the viewing angles of the instru-

ments affect the apparent brightness of the surface. As the emission angle increases, the amount of atmosphere through which the observations are collected increases. Atmospheric dust opacity increases as the atmospheric path length increases, and thus the observations can brighten without increase in the actual surface reflectivity as the emission angle increases. In addition, at larger emission angles, the surface phase function becomes non-Lambertian, further affecting comparison with the near-nadir MGS data.

[65] In Figure 28, we show plots of albedo difference (absolute and percentage) between IRTM and TES data for Viking year 1 and MGS mapping years 1 and 2 as a function of the maximum emission angle of Viking IRTM data used in the calculations, which we refer to as the IRTM "emission angle limit" or "limiting emission angle". The individual points on the plots are the mean results from different spatial bins of data collection in the southern mid and high latitudes. Different bins were used to eliminate potential data collection biases. The values for the individual bins are shown in Table 1. This table and Figure 28 show that after the end of the Viking year 1 and MGS mapping year 2 southern summer storm seasons (i.e., for the $L_s = 0 - 10°$ bins), the Viking southern mid and high latitudes are brighter than those observed by MGS. However, the magnitude of the brightness difference is seen to be a strong and consistent function of the IRTM emission angle. The Viking surface brightness excess falls from about 14% to 8% as the emission angle limit falls from $60°$ to $10°$. Relative to the global storm-free MGS mapping year 1 data, this brightness excess is about 18% at $60°$ limiting emission angle and

about 9–10% at 10° (again, the limiting emission angle is the highest emission angle allowed in the averaging; thus data from 0°–10° emission angle were allowed in the 10° limiting emission angle case). In this sense, the southern hemisphere observed by Viking at the turn of year 1 into year 2 was brighter than any of the MGS observations at this same seasonal date. However, as already stated above, the action of the seasonal ice cap retreat "cleaned" much of the southern and high latitudes after the 2001 storm, but not after the 1977b storm. If the surface is examined before the 1977b storm, the Viking southern mid and high latitudes are not as different. Figure 28 and Table 1 also show data for late southern spring ($L_s = 250°–260°$), for Viking year 1 and MGS years 1 (pre-2001 storm) and 2 (post-2001 storm). While the comparison with year 1 MGS data shows the southern hemisphere much brighter in the Viking data (presumably largely the effect of the 1977a storm), the MGS year 2 data suggest that the surface observed by MGS in the southern mid and high latitudes may actually have been brighter than observed by Viking at the same season. For both MGS years, the data again show the derived albedo to be a consistent function of emission angle. Viking brightness excess over MGS year 1 data drops from about 13% at 60° to about 8–9% at 10°. However, for MGS year 2, this difference drops from a 6% advantage for Viking at 60° to a 1% MGS brightness relative to Viking at 10° emission angle cut off.

[66] In all likelihood, then, the surface at $L_s = 250°–260°$ was actually brighter across the southern mid and high latitudes in MGS year 2 than in Viking year 1. Thus some fraction of the apparent brightness of the southern hemisphere during Viking relative to MGS is due to the broader range of emission angles, while much is associated with the particular time during the Viking and MGS missions that data were collected. The latter effect likely dominates the imaging comparison in Figure 24. In this sense, it is probably not strictly correct to say that a major Viking-to-MGS era change in surface albedo and dust cover is the darkening to the mid to high southern latitudes. While it is true that Figure 24 shows a "Viking era" surface in the high southern latitudes that is brighter (dustier) than an "MGS era" surface, this actually appears to result from the timing of the 1977b storm after the removal of the seasonal cap in the south. It also seems likely (on the basis of results shown in section 5) that much of the excess brightness of the southern mid and high latitudes would have subsided by late southern spring of Viking year 2, but unfortunately no Viking data exist to test this speculation.

[67] In short, comparison of surface brightness between missions appears to be dominated by the short-term history of dust storm activity (and their immediate aftermath) during the missions. Use of data such as shown in Figure 24 to assess long-term changes seems akin to sampling a time series at an interval much longer than the characteristic frequency of variation; changes on the timescale of individual storm events are aliased onto the sampling interval. There appears a particular danger of this for the surface dust record since the well-sampled TES albedo data shows that there is more variability on the former timescale than the latter (and hence more consistent intra-data set variation than inter-data set variation).

## 6.2. Northern Hemisphere Low-Albedo Patterns

[68] The second category of albedo changes between Viking and MGS involve modification of the shape and extent of low-albedo features in the otherwise high-albedo Tharsis, Amazonis, Arcadia, Utopia, Elysium, and Arabia regions. Changes in these regions relative to Viking have been noted by *Bell et al.* [1997], *Christensen et al.* [2001], *Caplinger and Malin* [2001], and *Geissler* [2005]. The latter provides detailed examination of several specific example locations. A collection of large low-albedo features exists in southern Utopia and Arcadia, and are shown in Figure 29 for Viking (the MDIM) and MGS (the geodesy campaign atlas [*Caplinger and Malin*, 2001]). Very substantial changes, especially for features in Hyblaeus and Cerberus (features c and e in Figure 29, respectively) occurred at some point between Viking and MGS, while these features have shown very little change during the MGS mission (see Figure 3). Since these low-albedo features disappeared (or nearly so) between the missions, the process of change has been deposition of dust, or the cessation of dust lifting. The areas of low albedo remaining in Cerberus take the form of dark wind streaks, suggesting that only in a very limited area have winds sufficient to lift dust been sustained. While the origin of these dark regions cannot be assessed directly from the available data, their sustained high albedo during the MGS mission suggests that seasonally varying winds are insufficient to have generated the low-albedo patterns observed by Viking and hence imply that abnormally high winds, likely associated with a dust storm (or storms) were responsible.

[69] Some of the features in this region remain similar between Viking and MGS, or show changes that are of a similar scale between the missions as are expressed within the MGS mission. Figure 30 shows the Viking MDIM view of two low-albedo features examined for the MGS data record in section 5.10. Comparison of the Viking data in Figure 30 with the MGS data in Figure 23 suggests that these features have not undergone significant secular change between the missions.

[70] Other low-albedo features observed by Viking within this broad region expanded between Viking and MGS. Examples examined by *Geissler* [2005] include the Nilosyrtis bright-dark boundary (area a in Figure 29) and Alcyonius (area b in Figure 29). *Geissler* [2005] notes that the boundary of dark surface in the northern hemisphere, which includes the portion in Nilosyrtis, has advanced southward over many decades, and that the Alcyonius low-albedo feature was absent in Mariner 9 observations. This suggests that the bright material in these locations is in some sense out of equilibrium, with the current balance of dust lifting versus depositional processes favoring lifting. An interesting question is what processes dominate the lifting/removal of dust? *Geissler* [2005] points to MOC narrow angle images of dust devil tracks within each of these regions and suggests on that basis that dust devils are the dominant form of dust erosion. This hypothesis carries with it a couple of major predictions: that the removal of material (darkening) should be a seasonally steady process, with the dust being steadily removed during the seasons of maximum dust devil activity; and, that there should be evidence of darkening of regions beyond that characterized by dramatic changes that can be associated with specific

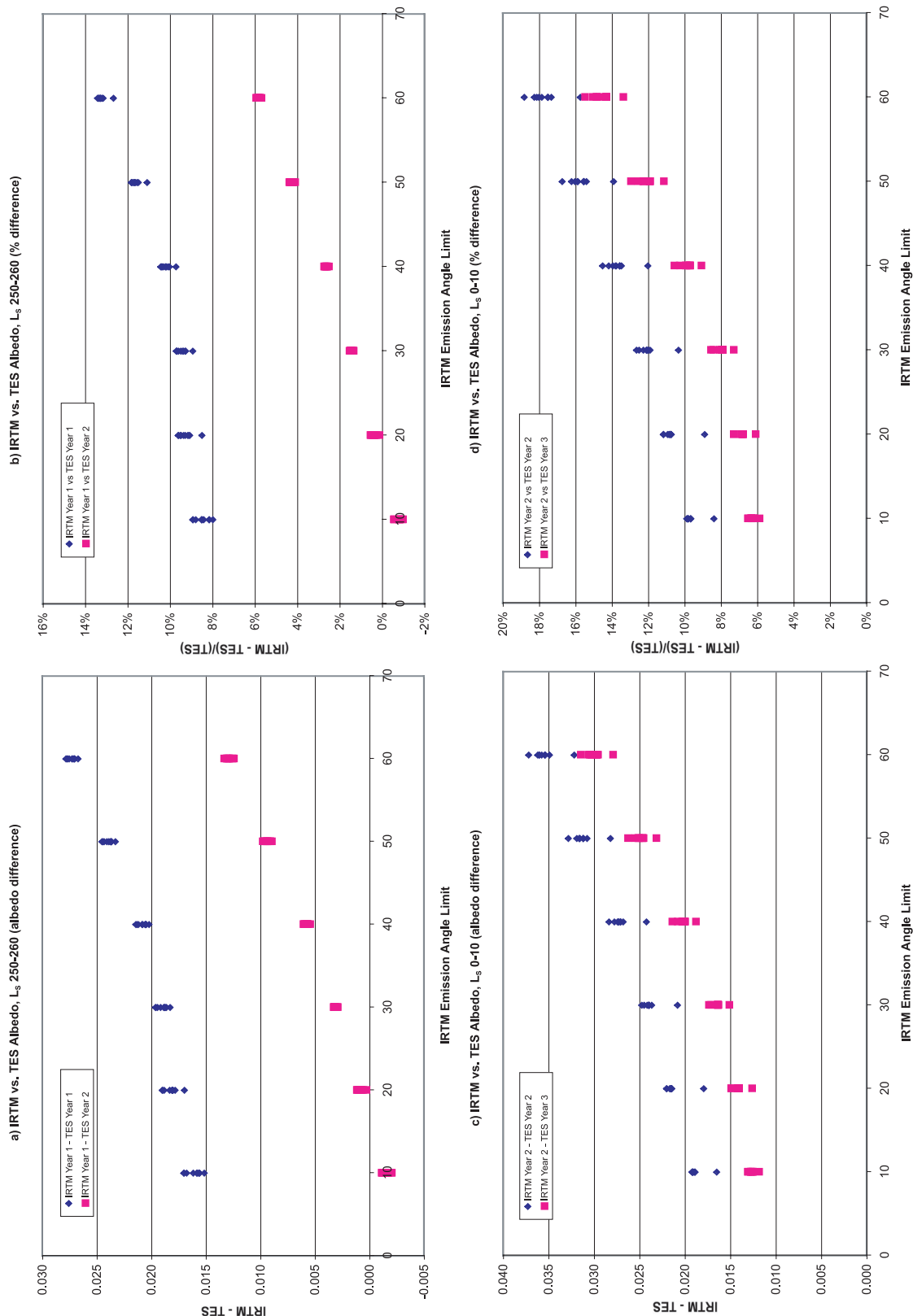**Figure 28.** Difference between IRTM and TES albedo (absolute and percentage) for Viking Year 1 and MGS mapping Years 1 and 2 as a function of the limiting emission angle of the IRTM data. Each point indicates a different area with good coverage in both IRTM and TES data that were randomly selected, with one point indicating a global average (see Table 1). Only bins that had data from IRTM Year 1, TES Year 1, and TES Year 2 were used.

**Table 1.** Measurement of Albedo Differences Between Two Years of TES Data and the First Year of IRTM Data as a Function of Location, Emission Angle, and Season[a]

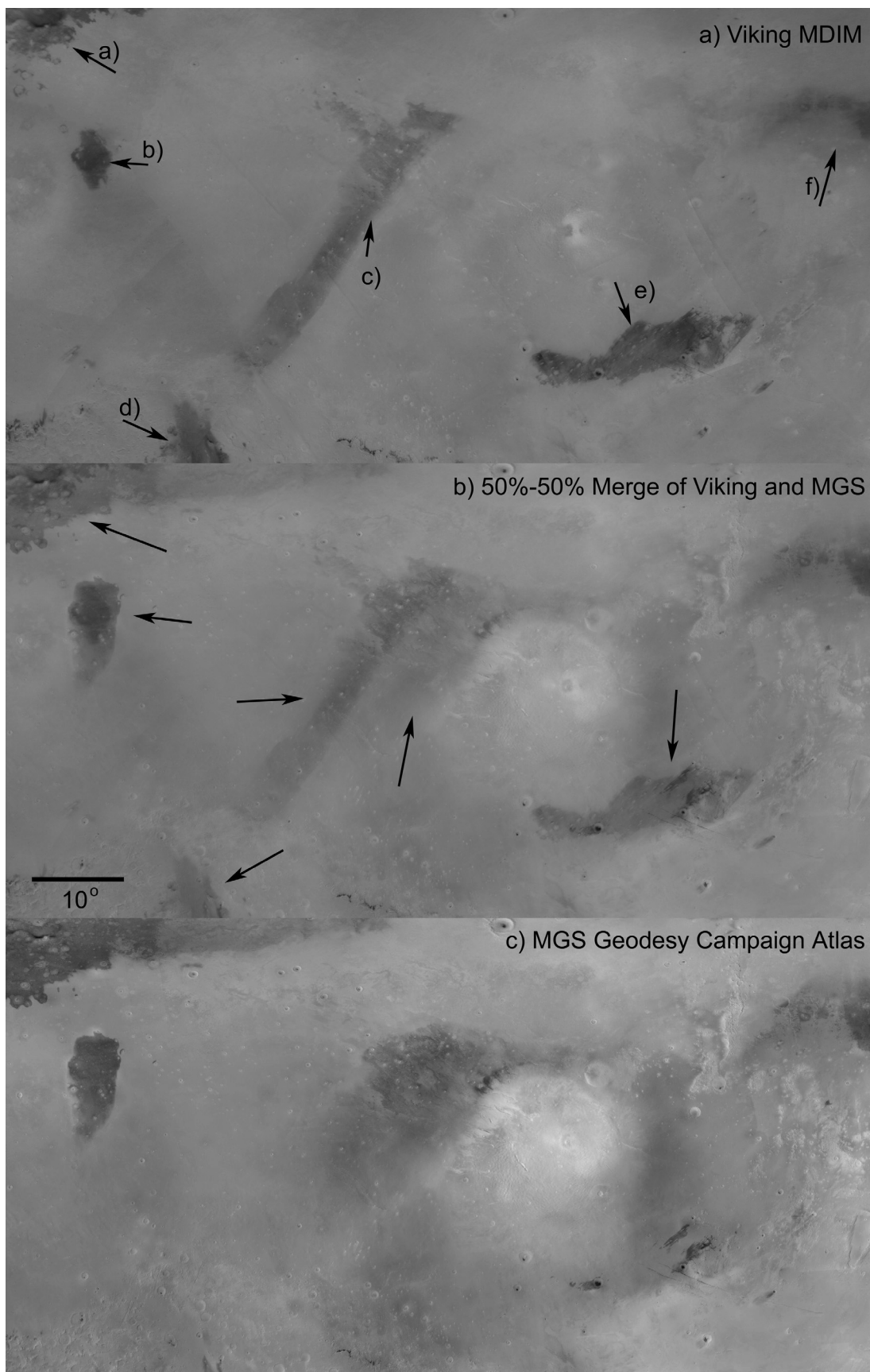| Latitude | | Longitude | | IRTM e< | $L_s = 250-260$ | | | | | | | $L_s = 0-10$ | | | | | | |
|---|---|---|---|---|---|---|---|---|---|---|---|---|---|---|---|---|---|---|
| Min | Max | Min | Max | | TES year 1 | TES year 2 | IRTM | IRTM − TES1 | % | IRTM − TES2 | % | TES year 2 | TES year 3 | IRTM | IRTM − TES1 | % | IRTM − TES2 | % |
| −90 | 90 | −180 | 180 | 60 | 0.2109 | 0.2243 | 0.2377 | 0.0267 | 12.66 | 0.0134 | 5.95 | 0.2045 | 0.2087 | 0.2366 | 0.0322 | 15.73 | 0.0279 | 13.38 |
| −50 | −40 | −180 | 180 | 60 | 0.2083 | 0.2231 | 0.2360 | 0.0277 | 13.27 | 0.0129 | 5.79 | 0.2020 | 0.2076 | 0.2374 | 0.0354 | 17.51 | 0.0297 | 14.32 |
| −80 | −60 | −150 | −120 | 60 | 0.2082 | 0.2229 | 0.2359 | 0.0277 | 13.33 | 0.0131 | 5.86 | 0.2020 | 0.2076 | 0.2374 | 0.0354 | 17.51 | 0.0297 | 14.32 |
| −80 | −60 | 90 | 120 | 60 | 0.2081 | 0.2227 | 0.2359 | 0.0278 | 13.37 | 0.0132 | 5.90 | 0.2020 | 0.2076 | 0.2374 | 0.0354 | 17.51 | 0.0297 | 14.32 |
| −80 | −25 | −180 | −110 | 60 | 0.2074 | 0.2217 | 0.2347 | 0.0273 | 13.15 | 0.0130 | 5.86 | 0.2013 | 0.2066 | 0.2362 | 0.0349 | 17.33 | 0.0296 | 14.32 |
| −40 | −20 | −180 | −110 | 60 | 0.2063 | 0.2207 | 0.2338 | 0.0275 | 13.34 | 0.0131 | 5.95 | 0.2002 | 0.2057 | 0.2360 | 0.0358 | 17.85 | 0.0303 | 14.70 |
| −60 | −15 | −110 | −70 | 60 | 0.2055 | 0.2198 | 0.2326 | 0.0271 | 13.20 | 0.0129 | 5.86 | 0.1998 | 0.2053 | 0.2358 | 0.0360 | 18.02 | 0.0305 | 14.85 |
| −45 | −8 | −50 | −10 | 60 | 0.2040 | 0.2186 | 0.2310 | 0.0270 | 13.26 | 0.0125 | 5.70 | 0.1987 | 0.2043 | 0.2347 | 0.0360 | 18.13 | 0.0304 | 14.86 |
| −40 | −45 | 5 | 35 | 60 | 0.2034 | 0.2179 | 0.2304 | 0.0270 | 13.29 | 0.0126 | 5.77 | 0.1980 | 0.2035 | 0.2342 | 0.0362 | 18.26 | 0.0307 | 15.06 |
| −25 | 0 | −50 | 0 | 60 | 0.2030 | 0.2177 | 0.2303 | 0.0272 | 13.41 | 0.0126 | 5.78 | 0.1976 | 0.2033 | 0.2348 | 0.0372 | 18.81 | 0.0315 | 15.49 |
| −90 | 90 | −180 | 180 | 30 | 0.2047 | 0.2199 | 0.2230 | 0.0183 | 8.92 | 0.0032 | 1.44 | 0.2013 | 0.2069 | 0.2221 | 0.0208 | 10.33 | 0.0151 | 7.32 |
| −50 | −40 | −180 | 180 | 30 | 0.2025 | 0.2190 | 0.2219 | 0.0194 | 9.60 | 0.0030 | 1.36 | 0.1994 | 0.2070 | 0.2234 | 0.0239 | 12.00 | 0.0164 | 7.92 |
| −80 | −60 | −150 | −120 | 30 | 0.2023 | 0.2187 | 0.2219 | 0.0196 | 9.67 | 0.0032 | 1.46 | 0.1994 | 0.2070 | 0.2234 | 0.0239 | 12.00 | 0.0164 | 7.92 |
| −80 | −60 | 90 | 120 | 30 | 0.2022 | 0.2186 | 0.2219 | 0.0196 | 9.70 | 0.0033 | 1.50 | 0.1994 | 0.2070 | 0.2234 | 0.0239 | 12.00 | 0.0164 | 7.92 |
| −80 | −25 | −180 | −110 | 30 | 0.2023 | 0.2180 | 0.2210 | 0.0187 | 9.26 | 0.0030 | 1.39 | 0.1987 | 0.2060 | 0.2224 | 0.0236 | 11.89 | 0.0163 | 7.93 |
| −40 | −20 | −180 | −110 | 30 | 0.2015 | 0.2171 | 0.2204 | 0.0189 | 9.35 | 0.0032 | 1.49 | 0.1983 | 0.2058 | 0.2222 | 0.0240 | 12.08 | 0.0164 | 7.96 |
| −60 | −15 | −110 | −70 | 30 | 0.2007 | 0.2161 | 0.2193 | 0.0186 | 9.27 | 0.0032 | 1.49 | 0.1980 | 0.2055 | 0.2220 | 0.0240 | 12.10 | 0.0164 | 7.99 |
| −45 | −8 | −50 | −10 | 30 | 0.1989 | 0.2146 | 0.2176 | 0.0187 | 9.41 | 0.0029 | 1.37 | 0.1968 | 0.2044 | 0.2209 | 0.0241 | 12.26 | 0.0165 | 8.08 |
| −40 | −45 | 5 | 35 | 30 | 0.1982 | 0.2138 | 0.2170 | 0.0188 | 9.49 | 0.0032 | 1.51 | 0.1958 | 0.2032 | 0.2203 | 0.0245 | 12.50 | 0.0171 | 8.44 |
| −25 | 0 | −50 | 0 | 30 | 0.1978 | 0.2136 | 0.2169 | 0.0191 | 9.68 | 0.0033 | 1.55 | 0.1957 | 0.2030 | 0.2204 | 0.0247 | 12.64 | 0.0174 | 8.57 |
| −90 | 90 | −180 | 180 | 10 | 0.1908 | 0.2089 | 0.2069 | 0.0162 | 8.47 | −0.0020 | −0.97 | 0.1967 | 0.2013 | 0.2132 | 0.0165 | 8.38 | 0.0119 | 5.89 |
| −50 | −40 | −180 | 180 | 10 | 0.1906 | 0.2094 | 0.2074 | 0.0168 | 8.79 | −0.0020 | −0.95 | 0.1955 | 0.2018 | 0.2144 | 0.0189 | 9.66 | 0.0126 | 6.23 |
| −80 | −60 | −150 | −120 | 10 | 0.1907 | 0.2094 | 0.2077 | 0.0170 | 8.91 | −0.0017 | −0.80 | 0.1955 | 0.2018 | 0.2144 | 0.0189 | 9.66 | 0.0126 | 6.23 |
| −80 | −60 | 90 | 120 | 10 | 0.1906 | 0.2093 | 0.2076 | 0.0170 | 8.92 | −0.0016 | −0.79 | 0.1955 | 0.2018 | 0.2144 | 0.0189 | 9.66 | 0.0126 | 6.23 |
| −80 | −25 | −180 | −110 | 10 | 0.1912 | 0.2085 | 0.2068 | 0.0156 | 8.15 | −0.0017 | −0.82 | 0.1950 | 0.2012 | 0.2140 | 0.0191 | 9.79 | 0.0128 | 6.36 |
| −40 | −20 | −180 | −110 | 10 | 0.1912 | 0.2085 | 0.2068 | 0.0156 | 8.15 | −0.0017 | −0.81 | 0.1949 | 0.2012 | 0.2140 | 0.0191 | 9.79 | 0.0128 | 6.34 |
| −60 | −15 | −110 | −70 | 10 | 0.1898 | 0.2061 | 0.2049 | 0.0151 | 7.98 | −0.0012 | −0.57 | 0.1949 | 0.2012 | 0.2140 | 0.0191 | 9.79 | 0.0128 | 6.34 |
| −45 | −8 | −50 | −10 | 10 | 0.1863 | 0.2035 | 0.2019 | 0.0157 | 8.41 | −0.0016 | −0.79 | 0.1949 | 0.2012 | 0.2140 | 0.0191 | 9.81 | 0.0128 | 6.34 |
| −40 | −45 | 5 | 35 | 10 | 0.1859 | 0.2028 | 0.2017 | 0.0158 | 8.51 | −0.0011 | −0.54 | 0.1945 | 0.2006 | 0.2137 | 0.0192 | 9.87 | 0.0131 | 6.53 |
| −25 | 0 | −50 | 0 | 10 | 0.1859 | 0.2028 | 0.2017 | 0.0158 | 8.51 | −0.0011 | −0.54 | 0.1945 | 0.2006 | 0.2137 | 0.0192 | 9.87 | 0.0131 | 6.53 |

aSee also Figure 28.

**Figure 29.** Images of some classical albedo features in the northern half of the eastern hemisphere. The image in Figure 29b shows the average brightness of Viking MDIM (shown in Figure 29a) and MGS Geodesy Campaign Atlas (shown in Figure 29c).
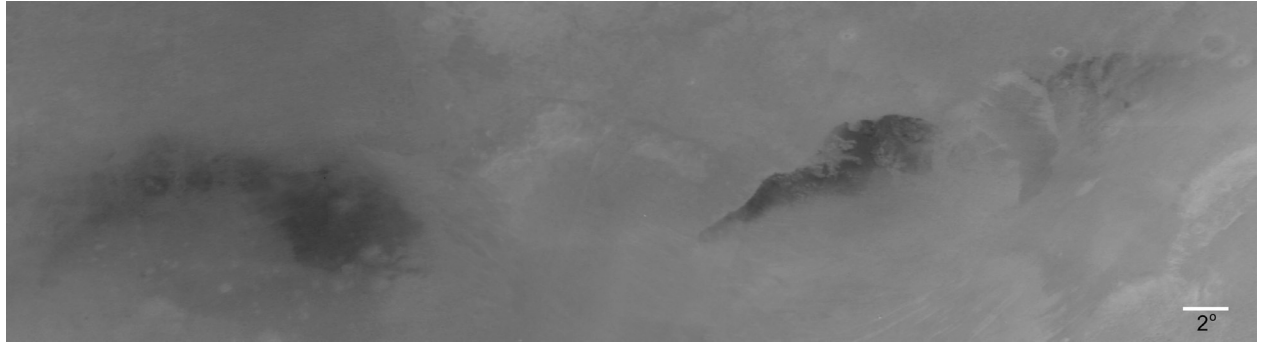
**Figure 30.** Viking MDIM view of two low-albedo features examined for the MGS data record in sections 5.9 and 5.10. See Figures 22 and 23 for MGS view.

meteorological events such as dust storms. The very high temporal resolution of the MOC DGM WA data allows us to test this hypothesis.

[71] *Geissler* [2005] has already shown that some of the shift in the position of the bright-dark boundary in Nilosyrtis occurred during the Viking mission, between 1978 and 1980, and also noted a subtle shift due to the 2001 storm. In Figure 31, we show portions of MOC DGM WA red images sampling most of the first three MGS mapping years. Between $L_s = 111°$ in year 1 (Figure 31a) and $L_s = 175°$ in year 2 (Figure 31c, just prior to the 2001 global storm), the shape and detailed pattern of the bright-dark boundary in Nilosyrtis is unchanged to the limiting resolution of the images. This includes the better part of two northern summers, when dust devil activity should have peaked at these latitudes [*Fisher et al.*, 2005]. By $L_s = 309°$ in year 2 (Figure 31d), after the atmospheric haze of the 2001 global dust storm had cleared, the formerly dark surfaces in Nilosyrtis appear to have become largely dust covered. While solar incidence angle is very high for this $L_s$, it is better than that for the year 3, $L_s = 291°$ image (Figure 31i), within which one can clearly recognize the bright-dark boundary. Further, a distinct dark region at the upper, center-left can be made out, suggesting that the apparent brightness of the surface across most of the region in this image represents widespread dust coverage. By $L_s = 73°$ (Figure 31e), in the late northern spring of the following year, most of the northern dark unit has been restored. It seems likely that frontal dust storms associated with low-pressure storm systems operating in the northern high latitudes in northern late winter and early spring [*Wang et al.*, 2003, 2005] were responsible for this "clean up" of dust deposited by the 2001 storm. This speculation is based on examination of images between those in Figures 31d and 31e. Specifically, the surface is obscured by what appear to be frontal aerosol clouds prior to image E1203464 at $L_s = 319°$ (about 10° of $L_s$ after Figure 31d). The $L_s = 319°$ image shows the bright dark boundary in the same configuration as in Figure 31e, for those parts of the image not obscured by atmospheric aerosol cloud (identified as such by its diffuse and streaky nature). There is ample additional evidence for atmospheric dust over the dark/bright boundary (and potentially dust lifting) in the image sequence from E1300040, E1300411, and E1301312 ($L_s = 319°$, 322°, and 328°, respectively). If not frontal storms, the action appears to be associated with a sporadic storm of

some type, and not by steady action. Adding to this is the fact that early mid northern winter is a highly unfavorable season for dust devil activity at these latitudes [*Fisher et al.*, 2005].

[72] Despite the approximate restoration of the dark-bright boundary to roughly its position before the 2001 global storm, in detail, the shape of the bright-dark boundary had changed from before the storm. Comparisons of Figures 31c and 31e show that some detailed dark features along the boundary were lost (dust covered) as a result of the storm (see area indicated by central arrow in Figure 31e). After the 2001 storm, and for the rest of the MGS mission until at least the start of mapping year 4, this boundary remained unchanged (compare Figures 31e and 31j). These observations show that the primary mode of modification of the bright-dark boundary location and shape in Nilosyrtis during the MGS missions was catastrophic, as opposed to gradual.

[73] The changes in the dark-bright boundary indicated in Figure 31 were associated with a brightening of a dark portion of the surface (an advance of the bright front). However, the majority of the change between Viking and MGS was an advance of the dark front. *Geissler* [2005] and *Fisher et al.* [2005] showed that the dark region behind the front has copious evidence for dust devils in the form of tracks. But does evidence of tracks imply a meaningful impact of dust devils on trends in the albedo of a large-scale region? This question can be directly addressed by examining the albedo trend in the region of heavy track coverage shown in Figure 32a (albedo data are shown for 45°N–55°N and 80°E–95°E; compare with Figure 8 of *Geissler* [2005]). In fact, this figure shows that during the MGS mission, there was no net trend in albedo for this region (only the spring and summer data is useful due to the influence of clouds and seasonal ice in northern autumn and winter). It is possible to convince oneself of a slight darkening trend across the spring and summer seasons, but it would seem that this is more plausibly ascribable to the clearing of dust from the atmosphere across this period (Figure 32b). On an annual basis, year 4 appears to be the brightest, along with the portion of year 1 observed, but this is may not be significant given the smallness of the signal (an albedo difference of maybe 0.005–0.01). These observations suggest that there is no steady trend or change in albedo for this region over an interval of greater than

**Figure 31.** Portions of MOC DGM WA red images of Nilosyrtis and Alcyonius (Thoth) sampling most of the first three MGS mapping years.
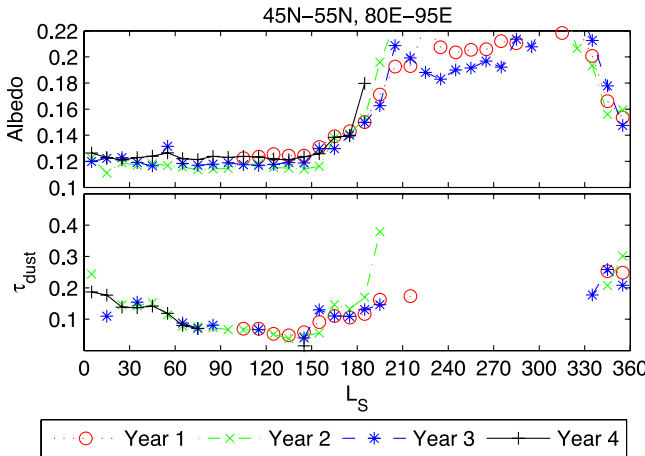
**Figure 32.** Similar to Figure 5 for part of Nilosyrtis (45°N–55°N, 80°E–95°E), but showing only albedo and dust infrared opacity.

three Martian years. This would appear contradictory to the expectation of steady clearing by dust devils. This is not to say that dust devils are not active in this region or cannot lift dust: their streaks litter the surface in MOC NA images [*Fisher et al.*, 2005; *Geissler*, 2005]. Instead, they simply appear inconsequential in effecting large-scale changes in albedo. Perhaps they simply redistribute dust on small scales within the low-albedo region, rather than exporting dust from the region? In any case, this contrasts sharply with the impact of global storms and short-term lifting events that produce very noticeable changes in the bright/dark boundary, as described in the previous paragraph.

[74] The Alcyonius low-albedo feature is also shown in Figure 31. Comparison of data collected between the beginning of the MGS mapping mission and the period immediately prior to the 2001 storm reveals no significant change in the shape and extent of this feature (compare Figures 31a–31c). After the storm (Figure 31d or more clearly in Figure 31e), some bright material was deposited in the southern portion of the feature during the 2001 storm or the storm fall-out. This brightening of the southern portion of the feature can also be seen in the TES data shown in Figure 3b. This material persists in the feature, and the shape and extent of the feature remain essentially constant, until northern autumn equinox of year 3 (Figure 31h). After $L_s = 210°$ in year 3, a large regional dust storm occurred (see Figures 1 and 25), after which the low-albedo feature in Alcyonius had changed in two ways (Figure 31i): the bright material in the southern portion of the feature was largely removed, and the southern boundary of the feature had become more elongated and sharpened. This change is especially evident in Figure 31j, collected just after northern spring equinox in year 4. A second regional dust storm after $L_s = 320°$ in year 3 did not appear to significantly modify the low-albedo feature (compare Figures 31i and 31j). The lack of steady changes in the extent and shape of this low-albedo feature in the northern springs and summers of years 1 to 3, combined with the clear association of rapid changes in the bound-

aries of this feature with major storm events again suggests that it is major dust storms rather than dust devils or any steady process that dictate the long-term modification of this feature.

## 7. Albedo Trends in Amazonis and Gusev Crater

[75] The role of dust devils in producing significant (in extent and duration) surface albedo variations can be examined further by looking at two sites: Amazonis Planitia, where the largest and most active dust devils have been observed from orbiter imaging [*Fisher et al.*, 2005], and Gusev crater, where the Spirit rover has observed copious dust devil activity (evident in publicly released images) and for which MOC and THEMIS imaging shows numerous dust devil streaks [*Greeley et al.*, 2003; *Toigo and Richardson*, 2003].

[76] *Fisher et al.* [2005] examined two different study areas in Amazonis. The larger region (25°N–45°N and 145°W–165°W) yielded by far the most dust devil observations in MOC WA and NA images of any study region examined. It was found that a specific subregion within Amazonis had been targeted for repeated WA imaging, centered at 36°N, 160°W and a few degrees on a side in each direction. Dust devil activity curves have been generated from this data set, illustrated in Figure 5 of *Fisher et al.* [2005], that show peak activity of roughly $2.5 \times 10^{-3}$ dust devils per km$^2$ in early northern summer (roughly $L_s = 120°$). Activity begins just before $L_s = 0°$ and terminates by $L_s = 190°$.

[77] The impact of this heavy dust devil activity on the albedo of both the larger and smaller Amazonis study regions is shown in Figure 33. For the larger study area, a modest darkening trend (about 0.01 of albedo) is observed across the spring and summers of three of the years shown (too little data is available from the first mapping year), however, this is associated with a similar reduction in the dust opacity, so it is not possible to uniquely ascribe the darkening to dust removal from the surface. On an interannual basis, the data show no change from year to year in the brightness of Amazonis, with the exception of a drop of maybe 0.01 between year 1 and the three subsequent years. Years 2–4 are indistinguishable. The albedo record for the smaller study region is noiser due to including fewer observations. Again, there is a hint of darkening through the active dust devil period, but again, this is mirrored in decreasing atmospheric dust optical depths. Also as evident for the larger area, there is no net interannual trend of albedo. To the level of noise, all four years are identical.

[78] Albedo and dust opacity data for the Gusev crater region (defined here as 13°S–16°S, 174°E–177°E) are shown in Figure 34. As with Amazonis, the albedo data are somewhat noisy due to the constrained sampling region. However, akin with Amazonis and Nilosyrtis (discussed in section 6.2), there is no net annual trend: the curves for each year lie on top of one another, to the level of the noise in the data. The combination of the Amazonis, Nilosyrtis, and Gusev data, for regions known to have either observed dust devil activity or dense dust devil tracks, suggests that even in regions where dust devils occur, they have no observable impact on large
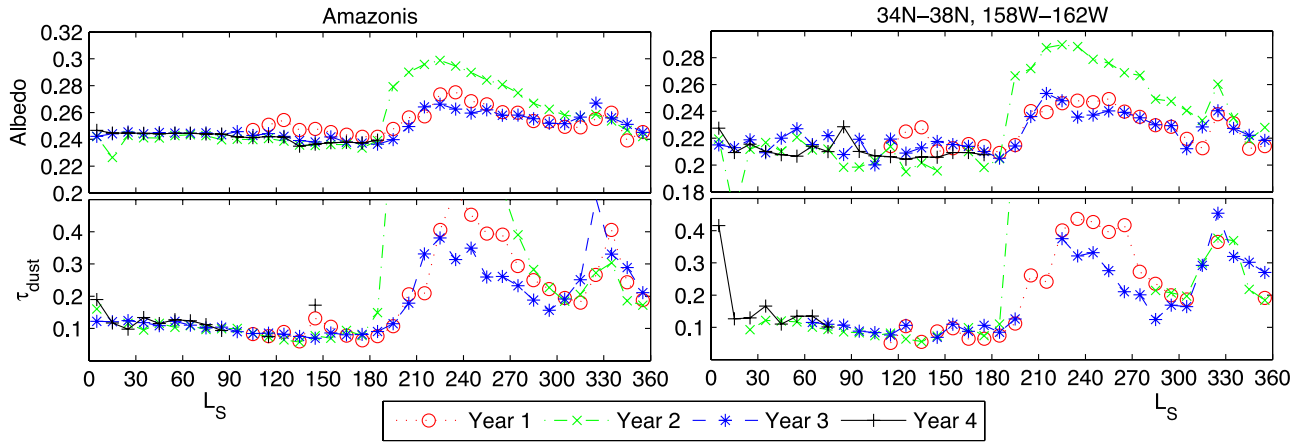
**Figure 33.** Similar to Figure 5 for both the larger Amazonis study area (25°N−45°N, 145°W−165°W) and smaller Amazonis study area (34°N−38°N, 158°W−162°W) [*Fisher et al.*, 2005], but showing only albedo and dust infrared opacity.

scale albedo over a time-base of a little over three Martian years.

## 8. Discussion

### 8.1. Processes

[79] In this study we hope to both document changes in the global distribution of surface dust and understand the processes involved by exploiting the temporal resolution of the TES albedo and MOC daily global map data sets. For example, candidate processes may be steady and ongoing, or "catastrophic" and punctuated. Indeed, the MGS data sets allow a detailed picture to be constructed of how the surface dust distribution is modified (e.g., section 5). As might be expected, major dust storms have a large impact on the surface dust distribution, most notably the 2001 GDS [*Smith et al.*, 2002; *Strausberg et al.*, 2005]. Sharp and unambiguous changes in the dust cover over an extended region in Daedalia provide clear evidence of a major dust source region for the 2001 storm that coincides with image evidence of strong lifting during the storm [*Strausberg et al.*, 2005]. The other observed major lifting center for the storm, the Hellas basin, shows a net increase of dust as a result of



**Figure 34.** Similar to Figure 5 for Gusev Crater (13°S−16°S, 174°E−177°E), but showing only albedo and dust infrared opacity.

the storm, suggesting that after the termination of this lifting center during the storm (some ten days or more before the end of lifting in Daedalia [*Strausberg et al.*, 2005]), Hellas became a sink for dust. However, the data show that the impact a GDS has varies regionally, with many locations showing no net effects. It is likely that dust lifting, immediate poststorm deposition, and gradual redistribution back to prestorm conditions (as speculated in section 5) may be a cyclical process.

[80] The post-2001 storm period illustrated several processes that allow darker surfaces that have been brightened by large storms to recover their prestorm albedos. In Syrtis, the substantial encroachment of dust immediately following the storm lasted only into the mid southern summer, whereupon the material was largely removed over a short period (several days) by the formation of wind streaks in the absence of observed dust storms. These observations are consistent with the idea that the seasonally varying regional winds in Syrtis reached a threshold for lifting in late summer and then rapidly accomplished the cleaning of Syrtis. If true, this suggests that some areas on Mars may be unable to sustain a dust cover due to the occurrence of widespread winds at some point in the year that exceed the threshold for dust lifting and removal.

[81] Another example of seasonally induced "cleansing" is provided in the high southern latitudes, where the recession of the southern seasonal ice cap was associated with the return of dust storm-brightened regions to their darker, prestorm appearance. In fact, the timing of the 1977b storm as compared with the 2001 storm may be largely responsible for the unusually bright southern high latitudes as illustrated in the Viking MDIM. While the latter storm began around southern spring equinox, the former commenced much later, near southern summer solstice, and after the vast majority of the southern seasonal ice cap for that year had sublimated. Data for the Viking MDIM were acquired in this southern summer period, but neither camera nor IRTM albedo data for the following summer was available. Given the ability of intensified wind systems associated with the southern seasonal cap edge (likely so-called "sea-breeze" circulations [*Siili*, 1996; *Toigo et al.*, 2002]) to clean storm-fall dust, we speculate that the following
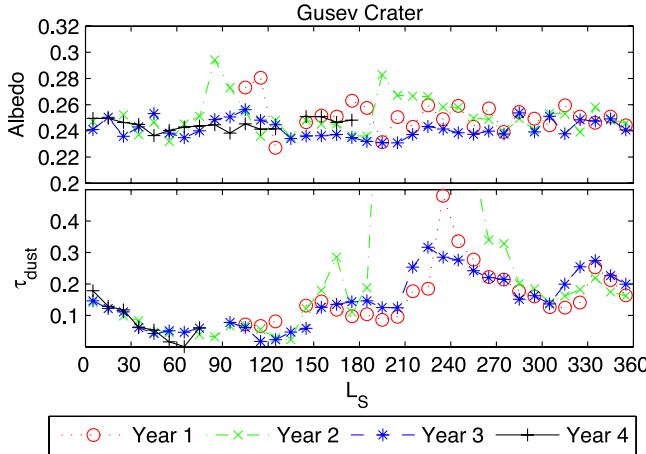
southern summer, much of the southern hemisphere would have been darkened to levels similar to those observed by MGS and hinted at in pre-1977 dust storm IRTM observations. As such, the very bright southern hemisphere observed by Viking appears to be an artifact of the storm timing, and may not reflect a decadal-scale evolution of the southern hemisphere dust distribution between the late 1970s and the late 1990s.

[82] In other locations, the albedo trends reflect the impact of multiple storms in the MGS record. Individual sites experiencing net loss of dust following one storm are observed to remain at the new albedo value until a subsequent storm rapidly repopulates the locale with dust. Some of the dark albedo features in the western northern midlatitudes, as well as the bright-dark boundary in the northern hemisphere, provide good examples of the impact of subsequent global, regional, and local dust storms.

[83] Despite the wide range of processes contributing to the redistribution of substantial surface dust, dust devils and other ongoing, small scale lifting processes do not appear to be among them. While it is possible to argue that such processes have a large and potentially dominant effect in the maintenance of the global background haze distribution [*Metzger et al.*, 1999; *Ferri et al.*, 2003; *Basu et al.*, 2004; *Fisher et al.*, 2005], such processes do not seem to provide the regional and local concentration of dust injection necessary to significantly alter the large-scale surface albedo on timescales of less than a few Martian years (the limit defined by the MGS baseline in this study of four Martian years). The images of dust devil streaks obtained by MOC simply do not appear to translate into steady changes in the large-scale surface albedo.

## 8.2. A Dust Cycle?

[84] While the term "dust cycle" is often used, it is not clear to what degree and on what timescales closure actually occurs. It has long been speculated that if dust storms preferentially export dust from certain source regions or latitudes, that some mechanism must return this material, and that the nature and timing of this return may play a role in the interannual variability of dust storms [e.g., *Haberle*, 1986]. For example, it is possible to construct idealized models of the dust cycle in which dust exported by major storms is resupplied by steady fall out of background haze, in turn lifted by dust devils or other ongoing processes. While the atmospheric branch of the dust cycle has been observed for many years, the net transport of dust is extremely difficult to even coarsely determine from these observations alone. The multiyear observations of albedo available from MGS allow new insight into the nature of the dust cycle.

[85] The observations described in section 5 suggest that dust is preferentially removed from certain regions during major storms. During the 2001 GDS, the major source region appears to have been south of Tharsis in Daedalia. Other regions appear to have gained substantial surface dust cover immediately following the storm. The observations further suggest that various mechanisms remove some of this material from sink locations, in some cases very quickly, within the same season or year. For Syrtis, the combined albedo and imaging data suggest that surface dust cover is unstable against regional winds in the late southern

summer, resulting in stripping of this cover through the development of mesoscale linear dark streaks that quickly merge, leaving only bright streaks in the lee of craters. In the mid and high southern latitudes, winds associated with the seasonal ice cap very effectively remove storm fallout surface dust. These observations suggest that many of the areas that are low albedo on Mars are dark because surface dust is unstable against large-scale wind erosion at wind speeds that readily occur at some point in the year. On the other hand, while there is copious evidence of removal of "unstable" dust cover following storms, there is less evidence of resupply of dust to Daedalia. However, an event or events that resupplied dust to Daedalia must have occurred between Viking and the start of the MGS mission, as the Viking and post-2001 dust storm dust distribution in the region south of Tharsis and in Daedalia are very similar.

[86] Taken in totality, the Viking and MGS data suggest that certain areas are more likely and certain areas are less likely to host surface dust (indeed, there may be something of a continuum of "stability"). Further, the dust cycle, such that it is, does not appear to consist of movement of dust from region A to region B, and then slowly back to A. Instead it appears to be much more complex and diverse, with individual small and large dust storm events moving dust between many different potential sites and on different timescales, depending on the nature of the individual storms and the particular pattern of available surface dust. As such, the system would appear to have a large number of degrees of freedom, with significant scope for history dependence. The latter may be very important as the dust fall out from one storm may require many different processes occurring on timescales from intraseasonal to multidecadal to be remobilized (e.g., compare the rapid removal of dust from Syrtis in 2001 versus the very slow southward retreat of the northern hemisphere bright region boundary, evident in Viking and MGS data. This clearly "unstable" dust was presumably laid down by a large storm prior to the first spacecraft observations.) Within this broad time window, other storms will occur, with different geographical patterns of net lifting/deposition. In some cases, these storms will be the agents of dust removal for dust that fell out following any number of previous storms. Thus no storm is operating on a "clean slate"; nor is it completely "cleaned up" before the onset of the next storm. If, as seems likely, the availability of surface dust is a major factor determining the evolution of dust storms, then this history dependence will have a significant feedback into the atmospheric branch of the dust cycle. For example, if the Daedalia surface dust were not available in 2001, would the storm in that year have been able to grow to global extent or to have lasted as long? In the following Martian year, a large storm developed in Chryse and propagated to the south and to the west, over Solis and Daedalia. This storm clearly lifted some of the limited amount of surface dust in Solis. Had the Daedalia surface dust that existed in early 2001 been available in 2003, would this storm have blown up to global scales?

[87] In short, the MGS and Viking albedo data do support the idea of a dust cycle, but one that is complex and diverse, with incomplete restoration following major dust storms, a very wide range of restoration timescales (that overlap the

timescales for additional storm events), and strong history dependence.

## 9. Summary

[88] We have drawn the following conclusions from our study of MGS and Viking albedo and imaging data:

[89] 1. On year-to-year timescales, surface albedo is an accurate proxy for surface dust coverage. This conclusion is supported by correlating surface albedo variations with atmospheric dust events and by comparing albedo with the spectrally derived Dust Cover Index [*Ruff and Christensen*, 2002].

[90] 2. Within any year, albedo changes due to dust redistribution must be differentiated from apparent changes introduced by observing the surface through seasonally varying atmospheric dust and water ice. Examination of the albedo and aerosol opacity trends across the more than three years of MGS data suggests that such differentiation is possible, especially on a regional basis, by comparing albedo trends with independent measures of atmospheric aerosols.

[91] 3. The TES albedo data provide an interpretable record of significant regional-scale changes in surface dust coverage. These changes occur and can persist over a wide variety of timescales (from days to years). To the extent that dust cover affects the climate through modification of surface heat and dust fluxes, albedo is an important and observable climatalogical variable for Mars, akin to sea-surface temperature data for Earth. While in retrospect this may seem obvious, to date albedo has been used simply as a fixed boundary condition in Mars climate models, not as a dynamic variable.

[92] 4. The degree of variability of surface dust cover (and the regional coherence) suggests that surface dust cover may provide an important "memory" site for the Martian climate system. While the atmosphere has a short time constant, the timescales of major redistribution of dust have been shown to extend from days to years. Again, this may support an analogic link with the heat reservoir provided by the uppermost layers of the oceans on the Earth. A two-way interaction occurs between the atmosphere and the ocean, with the latter effectively spreading the information content of the interaction to longer timescales than the atmosphere, by itself could support. The analogy prompts speculation about the role of the evolving surface dust distribution on Mars in the variability of large dust storms (and the circulation in general).

[93] 5. The examination of several areas of the surface in section 5 highlights the rich variety of processes affecting the surface dust distribution. Global storms have the most dramatic impact, but the persistence of the resultant perturbations in dust cover vary greatly from region to region. The background wind, winds associated with the seasonal ice cap edge, or local albedo contrasts, and frontal storms can play a significant role. Areas that were observed to be sources of dust early in a storm might not ultimately end up being net sources of dust integrated over the whole storm event. The recovery of dust cover in regions that are depleted by a storm appear to take longer to recover than many of the areas of net deposition by a large storm.

[94] 6. In several cases, the processes responsible for changes in dust coverage could be inferred from nearly global, daily imaging. The high spatial and temporal resolutions of the imagery were both crucial to make such interpretations. Important processes include dust storms with a wide range of length scales, winds associated with the seasonal cap edge, winds assumed to be associated with low-pressure cyclones, and regional wind systems. The latter, observed in Syrtis following the 2001 GDS, suggests that in some locations the background winds consistently exceed the threshold for dust lifting on a seasonal basis.

[95] 7. Dust devils or steady (continuous or ongoing) dust lifting processes do not appear to have a net annual impact on the surface dust distribution for the years observed by MGS.

[96] 8. The largest signal in the MGS albedo record is the 2001 GDS. Both a transient effect due to atmospheric dust loading and a secular change due to surface dust redistribution were observed. The Daedalia, Hellas, and Syrtis regions were notably affected. Daedalia appears to have been the largest net source of dust (as gauged from the magnitude of the sustained darkening), while Hellas (the location of the storm origin) substantially increased in brightness, suggesting it was a net dust sink over the life cycle of the storm. Syrtis experienced a substantial dust cover increase, but one that lasted only until late southern summer (see point 4).

[97] 9. Surface dust that is motile (i.e., that can be lifted and/or was recently deposited) appears to be the brightest, widespread, nonice material on Mars. The Tharsis region, which is part of the extensive high-albedo northern tropical dust continent, is sufficiently bright that the dust suspended during the 2001 GDS did not significantly increase the apparent albedo. However, following the storm, the albedo of Tharsis fell slightly, suggesting that a veneer of dust had been removed from the surface. By implication, the high-albedo continents may not be composed of uniform or equally motile dust.

[98] 10. The brightness of the southern hemisphere evident in the Viking MDIM [*McEwen and Soderblom*, 1993; *McEwen et al.*, 1993] relative to the MGS MOC geodesy campaign [*Caplinger and Malin*, 2001] and the MGS MOC cloud-free mosaic [*Geissler*, 2005] largely results from the occurrence of the 1977b GDS and its onset following the sublimation of the southern seasonal ice cap. The latter quickly cleans southern midlatitude and high-latitude surfaces of dust deposited by storms, but only if they occur early in the "dust storm season." Dust deposited by later storms, such as 1977b, will be cleaned by the cap the following year. The Viking MDIM was created from images acquired in the southern summer immediately following the storm and thus shows the southern hemisphere in a state when its albedo trend is near a local maximum. Albedo data from before the 1977a storm and from between the 1977 storms show the Viking-era southern mid and high latitudes to have similar albedo to that observed during MGS.

[99] 11. Differences in the shape and extent of low-albedo features within the northern tropical and midlatitude high-albedo continents between Viking and MGS are a result of dust storms that modify the surface over various length scales. The same appears to be true for the changing latitude of the northern-hemisphere bright-dark boundary (see section 6.2).

[100] 12. Major changes in dust cover on Mars appear to occur on relatively short (subseasonal) timescales (at least

for the period sampled by MGS, which provides the only high temporal resolution data set yet available). Thus long baseline (annual or multiannual) comparisons of "snapshots" are likely to alias this high-frequency variability onto the lower frequency defined by the sampling interval. This again argues for continuous (of order daily to a few degrees of $L_s$ interval) mapping of albedo/global imaging if the time series is to be properly observed.

[101]   13. The "cycle" of dust is complex in the sense that there is substantial regional variability in the participation of different geographical locations in different dust storm events, and in the rapidity (or activity) of other meteorological systems in "cleaning" or "restoring" regional dust cover. As a result, there is great geographic variability in the characteristic timescales of dust source availability and resupply. In this light, it seems likely that the abundantly varied montage of regional dust sources and sinks plays an important role in the evolution of individual storms (compare the 2001 global and 2003 regional storms) and more generally in the interannual variability of global dust storms.

[102]   14. Given the importance of surface dust to the dynamics of the atmosphere (through albedo and the availability of dust for lifting), these results further highlight the necessity of continuous, multiyear observations of the atmosphere and surface for understanding the dynamics of the dust cycle and its impact on the volatile cycles. This can be contrasted with the typical science requirement for Mars orbiters of one Martian year of observations.

# References

Balme, M. R., P. L. Whelley, and R. Greeley (2003), Mars: Dust devil track survey in Argyre Planitia and Hellas Basin, *J. Geophys. Res.*, *108*(E8), 5086, doi:10.1029/2003JE002096.

Basu, S., M. I. Richardson, and R. J. Wilson (2004), Simulation of the Martian dust cycle with the GFDL Mars GCM, *J. Geophys. Res.*, *109*, E11006, doi:10.1029/2004JE002243.

Bell, J. F., M. J. Wolff, P. B. James, R. T. Clancy, S. W. Lee, and L. J. Martin (1997), Mars surface mineralogy from Hubble Space Telescope imaging during 1994–1995: Observations, calibration, and initial results, *J. Geophys. Res.*, *102*(E4), 9109–9123.

Bell, J. F., M. J. Wolff, T. C. Daley, D. Crisp, P. B. James, S. W. Lee, J. T. Trauger, and R. W. Evans (1999), Near-infrared imaging of Mars from HST: Surface reflectance, photometric properties, and implications for MOLA data, *Icarus*, *138*(1), 25–35.

Cantor, B. A., P. B. James, M. Caplinger, and M. J. Wolff (2001), Martian dust storms: 1999 Mars Orbiter Camera observations, *J. Geophys. Res.*, *106*(E10), 23,653–23,687.

Capen, C. F. (1976), Martian albedo feature variations with season—Data of 1971 and 1973, *Icarus*, *28*(2), 213–230.

Caplinger, M. A., and M. C. Malin (2001), Mars Orbiter Camera geodesy campaign, *J. Geophys. Res.*, *106*(E10), 23,595–23,606.

Christensen, P. R. (1986), Regional dust deposits on Mars: Physical properties, age, and history, *J. Geophys. Res.*, *91*(B3), 3533–3545.

Christensen, P. R. (1988), Global albedo variations on Mars: Implications for active aeolian transport, deposition, and erosion, *J. Geophys. Res.*, *93*(B7), 7611–7624.

Christensen, P. R., et al. (2001), Mars Global Surveyor Thermal Emission Spectrometer experiment: Investigation description and surface science results, *J. Geophys. Res.*, *106*(E10), 23,823–23,872.

Clancy, R. T. (2000), An intercomparison of ground-based millimeter, MGS TES, and Viking atmospheric temperature measurements: Seasonal and interannual variability of temperatures and dust loading in the global Mars atmosphere, *J. Geophys. Res.*, *105*(E4), 9553–9571.

Clancy, R. T., A. W. Grossman, M. J. Wolff, P. B. James, D. J. Rudy, Y. N. Billawala, B. J. Sandor, S. W. Lee, and D. O. Muhleman (1996), Water vapor saturation at low altitudes around Mars aphelion: A key to Mars climate?, *Icarus*, *122*(1), 36–62.

Ferri, F., P. H. Smith, M. Lemmon, and N. O. Rennó (2003), Dust devils as observed by Mars Pathfinder, *J. Geophys. Res.*, *108*(E12), 5133, doi:10.1029/2000JE001421.

Fisher, J. A., M. I. Richardson, C. E. Newman, M. A. Szwast, C. Graf, S. Basu, S. P. Ewald, A. D. Toigo, and R. J. Wilson (2005), A survey of Martian dust devil activity using Mars Global Surveyor Mars Orbiter Camera images, *J. Geophys. Res.*, *110*, E03004, doi:10.1029/2003JE002165.

Geissler, P. E. (2005), Three decades of Martian surface changes, *J. Geophys. Res.*, *110*, E02001, doi:10.1029/2004JE002345.

Greeley, R., N. Lancaster, S. Lee, and P. Thomas (1992), Martian aeolian processes, sediments, and features, in *Mars*, edited by H. H. Kieffer et al., pp. 730–766, Univ. of Ariz. Press, Tucson.

Greeley, R., R. O. Kuzmin, S. C. R. Rafkin, T. I. Michaels, and R. Haberle (2003), Wind-related features in Gusev crater, Mars, *J. Geophys. Res.*, *108*(E12), 8077, doi:10.1029/2002JE002006.

Haberle, R. M. (1986), Interannual variability of global dust storms on Mars, *Science*, *234*(4775), 459–461.

James, P. B., J. F. Bell, R. T. Clancy, S. W. Lee, L. J. Martin, and M. J. Wolff (1996), Global imaging of Mars by Hubble Space Telescope during the 1995 opposition, *J. Geophys. Res.*, *101*(E8), 18,883–18,890.

Kahn, R. A., T. Z. Martin, R. W. Zurek, and S. W. Lee (1992), The Martian dust cycle, in *Mars*, edited by H. H. Kieffer et al., pp. 1017–1053, Univ. of Ariz. Press, Tucson.

Lecacheux, J., P. Drossart, C. Buil, P. Laques, E. Thouvenot, and P. Guerin (1991), CCD images of Mars with the 1 M reflector atop Pic-Du-Midi, *Planet. Space Sci.*, *39*(1–2), 273–279.

Lee, S. W. (1986), Regional sources and sinks of dust on Mars: Viking observations of Cerberus, Solis Planum, and Syrtis Major, in *Symposium on Mars: Evolution of Its Climate and Atmosphere, LPI Contrib. 599*, p. 57, Lunar and Planet. Inst., Houston, Tex.

Liu, J., M. I. Richardson, and R. J. Wilson (2003), An assessment of the global, seasonal, and interannual spacecraft record of Martian climate in the thermal infrared, *J. Geophys. Res.*, *108*(E8), 5089, doi:10.1029/2002JE001921.

Malin, M. C., and K. S. Edgett (2001), Mars Global Surveyor Mars Orbiter Camera: Interplanetary cruise through primary mission, *J. Geophys. Res.*, *106*(E10), 23,429–23,570.

Malin, M. C., G. E. Danielson, A. P. Ingersoll, H. Masursky, J. Veverka, M. A. Ravine, and T. A. Soulanille (1992), Mars Observer Camera, *J. Geophys. Res.*, *97*(E5), 7699–7718.

Martin, L. J., and R. W. Zurek (1993), An analysis of the history of dust activity on Mars, *J. Geophys. Res.*, *98*(E2), 3221–3246.

McEwen, A. S., and L. A. Soderblom (1993), Global and regional/seasonal color mosaics of Mars, *Proc. Lunar Planet. Sci. Conf. 25th*, 953–954.

McEwen, A. S., L. A. Soderblom, T. L. Becker, E. M. Lee, and R. M. Batson (1993), Global color views of Mars, in *Lunar and Planetary Inst., Mars: Past, Present, and Future, LPI Tech. Rep. 93–06*, Part 1, p. 29, Lunar and Planet. Inst., Houston, Tex.

McKim, R. (1999), Telescopic Martian dust storms: A narrative and catalogue, *Mem. Br. Astron. Assoc.*, *44*, 1–168.

Metzger, S. M., J. R. Carr, J. R. Johnson, T. J. Parker, and M. T. Lemmon (1999), Dust devil vortices seen by the Mars Pathfinder camera, *Geophys. Res. Lett.*, *26*(18), 2781–2784.

Pankine, A. A., and A. P. Ingersoll (2004), Interannual variability of Mars global dust storms: An example of self-organized criticality?, *Icarus*, *170*(2), 514–518.

Pearl, J. C., M. D. Smith, B. J. Conrath, J. L. Bandfield, and P. R. Christensen (2001), Observations of Martian ice clouds by the Mars Global Surveyor Thermal Emission Spectrometer: The first Martian year, *J. Geophys. Res.*, *106*(E6), 12,325–12,338.

Pleskot, L. K., and E. D. Miner (1981), Time variability of Martian bolometric albedo, *Icarus*, *45*(1), 179–201.

Pollack, J. B., E. H. Greenberg, and C. Sagan (1967), A statistical analysis of Martian wave of darkening and related phenomena, *Planet. Space Sci.*, *15*(5), 817–827.

Richardson, M. I. (1998), Comparison of microwave and infrared measurements of Martian atmospheric temperatures: Implications for short-term climate variability, *J. Geophys. Res.*, *103*(E3), 5911–5918.

Ruff, S. W., and P. R. Christensen (2002), Bright and dark regions on Mars: Particle size and mineralogical characteristics based on Thermal Emission Spectrometer data, *J. Geophys. Res.*, *107*(E12), 5127, doi:10.1029/2001JE001580.

Sagan, C., J. Veverka, P. Fox, R. Dubisch, J. Lederberg, E. Levinthal, L. Quam, R. Tucker, J. B. Pollack, and B. A. Smith (1972), Variable features on Mars: Preliminary Mariner 9 television results, *Icarus*, *17*(2), 346–372.

Sagan, C., et al. (1973), Variable features on Mars: 2. Mariner 9 global results, *J. Geophys. Res.*, *78*(20), 4163–4196.

Siili, T. (1996), Modeling of albedo and thermal inertia induced mesoscale circulations in the midlatitude summertime Martian atmosphere, *J. Geophys. Res.*, *101*(E6), 14,957–14,968.

Smith, M. D. (2004), Interannual variability in TES atmospheric observations of Mars during 1999–2003, *Icarus*, *167*(1), 148–165.

Smith, M. D., J. C. Pearl, B. J. Conrath, and P. R. Christensen (2000), Mars Global Surveyor Thermal Emission Spectrometer (TES) observations of dust opacity during aerobraking and science phasing, *J. Geophys. Res.*, *105*(E4), 9539–9552.

Smith, M. D., R. J. Conrath, J. C. Pearl, and P. R. Christensen (2002), Thermal Emission Spectrometer observations of Martian planet-encircling dust storm 2001A, *Icarus*, *157*(1), 259–263.

Strausberg, M. J., H. Wang, M. I. Richardson, S. P. Ewald, and A. D. Toigo (2005), Observations of the initiation and evolution of the 2001 Mars global dust storm, *J. Geophys. Res.*, *110*, E02006, doi:10.1029/2004JE002361.

Thomas, P. C., P. Gierasch, R. Sullivan, D. S. Miller, E. A. Del Castillo, B. Cantor, and M. T. Mellon (2003), Mesoscale linear streaks on Mars: Environments of dust entrainment, *Icarus*, *162*(2), 242–258.

Toigo, A. D., and M. I. Richardson (2003), Meteorology of proposed Mars Exploration Rover landing sites, *J. Geophys. Res.*, *108*(E12), 8092, doi:10.1029/2003JE002064.

Toigo, A. D., M. I. Richardson, R. J. Wilson, H. Wang, and A. P. Ingersoll (2002), A first look at dust lifting and dust storms near the south pole of Mars with a mesoscale model, *J. Geophys. Res.*, *107*(E7), 5050, doi:10.1029/2001JE001592.

Veverka, J. (1975), Variable features on Mars 5: Evidence for crater streaks produced by wind erosion, *Icarus*, *25*(4), 595–601.

Veverka, J. (1976), Variable features on Mars 7: Dark filamentary markings on Mars, *Icarus*, *27*(4), 495–502.

Veverka, J., C. Sagan, L. Quam, R. Tucker, and B. Eross (1974), Variable features on Mars 3: Comparison of Mariner 1969 and Mariner 1971 photography, *Icarus*, *21*(3), 317–368.

Wang, H., and A. P. Ingersoll (2002), Martian clouds observed by Mars Global Surveyor Mars Orbiter Camera, *J. Geophys. Res.*, *107*(E10), 5078, doi:10.1029/2001JE001815.

Wang, H., M. I. Richardson, R. J. Wilson, A. P. Ingersoll, A. D. Toigo, and R. W. Zurek (2003), Cyclones, tides, and the origin of a cross-equatorial dust storm on Mars, *Geophys. Res. Lett.*, *30*(9), 1488, doi:10.1029/2002GL016828.

Wang, H., R. W. Zurek, and M. I. Richardson (2005), Relationship between frontal dust storms and transient eddy activity in the northern hemisphere of Mars as observed by Mars Global Surveyor, *J. Geophys. Res.*, *110*, E07005, doi:10.1029/2005JE002423.

———————————

M. I. Richardson and M. A. Szwast, Division of Geological and Planetary Sciences, California Institute of Technology, MS 150-21, Pasadena, CA 91125, USA. (mir@gps.caltech.edu)

A. R. Vasavada, Jet Propulsion Laboratory, California Institute of Technology, 4800 Oak Grove Drive, Pasadena, CA 91109, USA.